BRNO UNIVERSITY OF TECHNOLOGY
VYSOKÉ UČENÍ TECHNICKÉ V BRNĚ

FACULTY OF ELECTRICAL ENGINEERING AND COMMUNICATION
FAKULTA ELEKTROTECHNIKY
A KOMUNIKAČNÍCH TECHNOLOGIÍ

DEPARTMENT OF MICROELECTRONICS
ÚSTAV MIKROELEKTRONIKY

HIGH EFFICIENCY N-TYPE MONOCRYSTALLINE SILICON SOLAR CELLS
SOLÁRNÍ ČLÁNKY Z MONOKRYSTALICKÉHO KŘEMÍKU TYPU N S VYSOKOU ÚČINNOSTÍ

DOCTORAL THESIS
DIZERTAČNÍ PRÁCE

AUTHOR — Ing. Barbora Mojrová
AUTOR PRÁCE

SUPERVISOR — prof. Ing. Jaroslav Boušek, CSc.
ŠKOLITEL

BRNO 2019

KLÍČOVÁ SLOVA

Solární článek, křemík, n-typ, bórový emitor, difuze, pasivační vrstva, metalizace.

KEY WORDS

Solar cell, silicon, *n*-type, boron emitter, diffusion, passivation layer, metallization.

LOCATION OF THE THESIS

Brno University of Technology, Faculty of Electrical Engineering and Communication, Department of Microelectronics, Technická 3058/10, 616 00 Brno, Czech Republic.

CONTENT

INTRODUCTION

This work is dedicated to the high-efficiency monocrystalline solar cells based on the *n*-type silicon, which seems to be more promising material for further investigation than the standard *p*-type material, because *n*-type substrates are, among other things, less prone to various degradation mechanisms occurring here on Earth. This advantage transfers directly into reliability and lifetime performance. The ambition of this dissertation thesis was to increase the efficiency and to it related parameters of *n*-PERT solar cell (*n*-type based solar cell with Passivated Emitter, Rear Totally Diffused).

Most of the experimental work took place at the International Solar Energy Research Center in Konstanz (ISC Konstanz) in Germany where a pilot-scale manufacturing line for production of solar cells in various types, including technologies based on both – *p*-type and *n*-type material, is placed. Research teams at the ISC Konstanz are focused on developing of methods leading to increase efficiency of solar cells manufactured at standard industrial devices, which have been mostly set up for *p*-type-based production. The production line there is based on batch processes. The topography pictures of solar cells surface were taken at Fill Factory (formerly Solartec) in Rožnov pod Radhoštěm.

1 ADVANTAGES OF *N*-TYPE SOLAR CELLS

Despite the rapidly increasing number of materials and technologies used for solar cell production the silicon and silicon-based technology stays as the photovoltaics mainstream. This is due to good electrical properties of silicon and also an established technology of electrical components production from silicon (Si). The technologies featuring the highest efficiencies in the industrial production are based on *n*-type Czochralski (Cz) silicon wafers. There is an overview of main advantages of using the *n*-type silicon instead of the *p*-type:

Due to the absence of boron there is no light induced degradation (LID) occurring in the *p*-type silicon wafers, caused by boron-oxygen complexes. The LID in the *p*-type solar cells occurs when oxygen impurities in the silicon wafer react with the doped boron in the first few hours/weeks of an illumination of the cell. This effect causes degradation in the carrier lifetime and immediately reduces cell efficiencies by 2 % - 4 %. The absence of boron in phosphorus-doped *n*-type substrates eliminates the boron oxygen defects even for the higher oxygen concentration and thus this drop in efficiency and power output is not evident [1] [2].

The *n*-type silicon is less sensitive to prominent metallic impurities, such as the interstitial iron (Fe), which can capture electrons much more effectively as it has a positive charge. The minority carriers in the *n*-type silicon are holes instead of electrons, as in the case of the *p*-type silicon. Therefore, it offers a higher minority carrier diffusion length in comparison to the *p*-type crystalline silicon wafers with similar impurity concentrations [3] [4] [5].

The fabrication of solar cells with an efficiency of over 20 % requires wafers with high electrical quality. However, producers of the *n*-type cells can rely on using lower quality and thus cheaper wafers (in particular thanks to the higher minority charge carrier diffusion length) [6].

The use of a phosphorus-doped back surface field (BSF) with convenient surface passivation for such *n*-type cells results in a higher diffusion length and better rear internal reflection. The use of a boron-doped front emitter with a rear side phosphorus-doped BSF on *n*-type substrates offers a bifacial type cell structure which can be fabricated on thinner wafers. Convenience of making such bifacial designed solar cells and modules using phosphorus-doped BSF also generates opportunities to produce cells with higher efficiencies [5].

There is the evidence that the *n*-type devices are more sensitive to a low light intensity, as well as having a lower temperature coefficient, mostly due to a higher V_{OC}. Also, the *n*-type silicon is less prone to degradation during high temperature processes, e.g. boron diffusion [5] [7].

Based on these advantages the *n*-type seems to be highly suitable for advanced high efficiency cell concepts like interdigitated back contact cells and passivated emitter and rear cell/locally diffused type cells, as well as bifacial passivated emitter and rear totally diffused type cells, which are described in the following chapter.

1.1 PERT CONCEPT OF SOLAR CELL

The PERT (Passivated Emitter, Rear Totally Diffused, **Fig. 1**) cell concept can be easily modified to *n*-type substrates and offers a high efficiency potential. It can be fabricated with the front emitter or as back junction cells with the emitter on the rear side. The company Imec announced that they have realized bifacial *n*-PERT solar cells using an industrially-compatible process with an average front-side conversion efficiency of 22.4 %, with the best cell topping 22.8 %. Under standard front illumination conditions in conjunction with an additional 0.15 sun rear illumination these bifacial cells can produce energy equivalent to 26.2 % at monofacial cells [8].

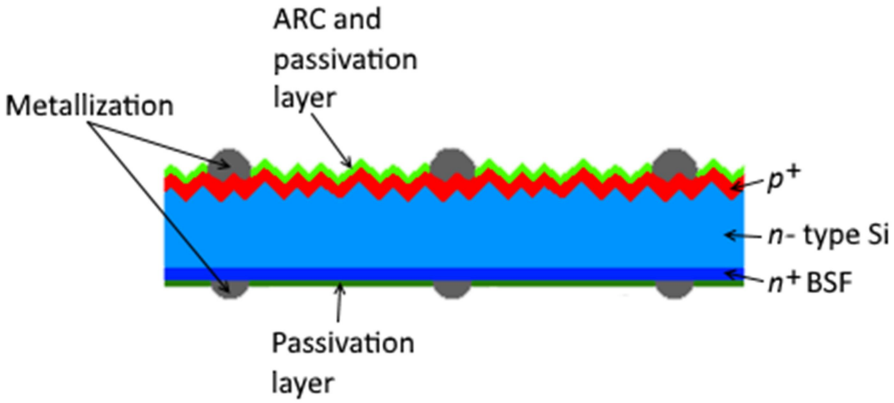

Fig. 1: Schematic drawing of *n*-PERT solar cell.

1.2 STANDARD PROCESS FLOW

The majority of industrially produced crystalline silicon solar cells are fabricated from multicrystalline (mc-Si) and monocrystalline (mono-Si) grown silicon wafers due to lower production cost and the potential for higher efficiencies. The main process steps in production of solar cells from silicon in industry highly resemble each other. It begins with treatment of bare silicon wafers, continues with boron/phosphorus diffusions and depositions of ARC and passivation layers, and finishes with metallization. The typical production process of *n*-type PERT crystalline silicon solar cells, used in solar cell industry, is characterised by a limited number of process steps, which are shown in **Fig. 2**.

a) saw damage etching and cleaning

b) phosphorous diffusion to create n^+ back surface field

c) deposition of passivation layer on the rear side

d) texturization and cleaning

e) boron diffusion to create p^+ emitter

f) deposition of antireflection and passivation layer on the front side

g) screen printing metallization, drying and firing

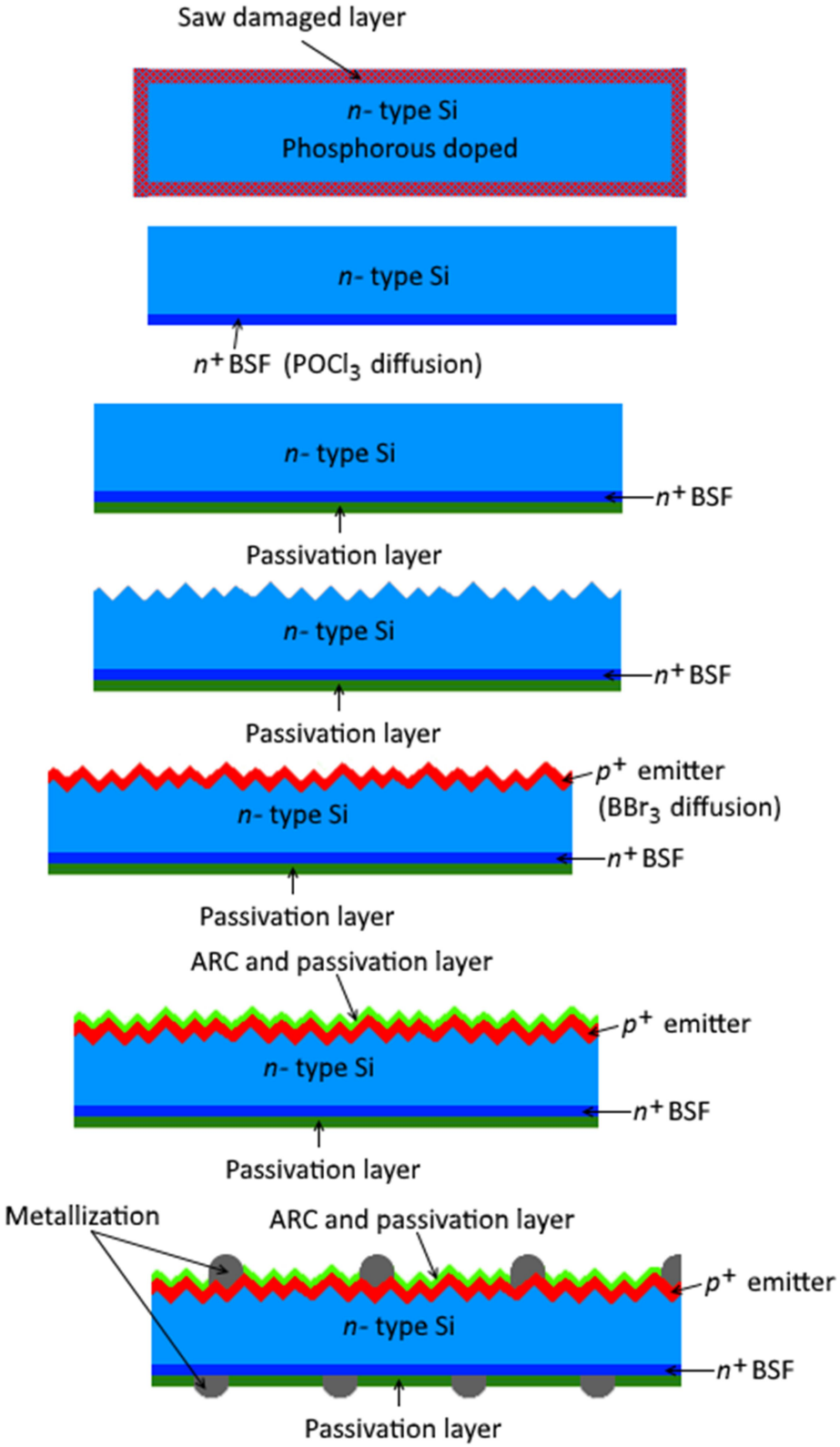

Fig. 2: Standard industrial *n*-PERT solar cell manufacturing process.

2 GOALS OF DISSERTATION

The goal of this work was to prepare high efficiency photovoltaic cells based on the *n*-type monocrystalline silicon substrate using the standard production line, which have originally been designed for production on *p*-type substrates. This approach encounters problems caused by different material parameters of the *n*-type substrate comparing with the *p*-type substrate. Therefore, this enhances new structures that need a new approach in use of standard or new materials and their combinations. Resulting cells could be used in standard as well as advanced bifacial applications.

The production of a photovoltaic cell consists of many steps, which often influence one another. Therefore, for the successful development of the solar cells structure using the *n*-type substrate and implementation of new particular process steps leading to the high efficiency solar cells it is indispensable to reach following goals in technology design and validation.

1) New ways of diffusion and oxidation processes:

   Selection between available types of diffusion processes is therefore needed and the influence of both dry oxidation and wet oxidation processes should be studied. Evaluation of possible interactions between diffusion and oxidation processes is indispensable. Also the influence of low pressure and atmospheric pressure boron diffusion on resulting parameters of the cells should be investigated.

2) Design of the optimal structure of passivation layers and antireflective coating:

   The properties of SiO_2 or BSG layers serving as the separating layer between SiN_X and the boron emitter and their optimal thickness must be investigated and thereafter ensured. The dependence of refractive index on stoichiometry of deposited layers, density of the layers and interface states, as well as the amount of positive interface fix charges on respective process parameters and on the deposition rate must be investigated.

   Special attention should be paid to creating an n^+ BSF layer prepared by phosphorus diffusion. Passivation SiN_X layer has here the same function as on the front side. Nevertheless, both SiN_X layers, for the front and the rear side, will have different parameters. Therefore two deposition processes, that is, for the front and rear side must be investigated.

3) Minimization of energy losses caused by contact resistance

   The temperature required for burning through the passivation and ARC layer could be derived by in-situ resistance measurements and from the resistance profile which results from resistance measurements. The goal is to record resistance changes during firing of metallization under different conditions and determine the temperature required for burning through the dielectric layer.

Apart from the composition of contact material also influence of oxygen concentration during the firing process must be well explored.

4) Minimization of the short-circuit effects

   For suppression of short circuit effects, the attention must be paid to the processes taking place during the contact firing, to surface topographies of the contacts, to thickness of SiN_X layer and also to doping concentration and doping profile.

5) PID prevention at the solar cell level

   To ensure the reliability of prepared photovoltaic cells and their durability in solar panels, cell protection with respect to the Potential Induced Degradation (PID) must also be addressed. As an addition to the above-mentioned technological steps ensuring high cell efficiency here the results are important in practical use of the cells. There it is necessary to determine how the PID effect is influenced by the composition of ARC and passivation layers, by the concentration profile of boron emitter and by the type of the surface texture.

3 RESULTS

3.1 DIFFUSION AND OXIDATION PROCESSES

3.1.1 Optimization of emitter doping profile

To find an optimal shape of the boron emitter doping profile for screen-printed solar cells, we created 6-inch *n*-PERT solar cells shown in **Fig. 3**. For this study, boron emitters with different emitter doping profile (**Fig. 4**) and resulting sheet resistance R_{Sh} were realized to see which parameter had more significant influence on final parameters of the solar cell. The maximum deviation of sheet resistance did not exceed 5 %, which is one of the requirements needed for good quality of metallization.

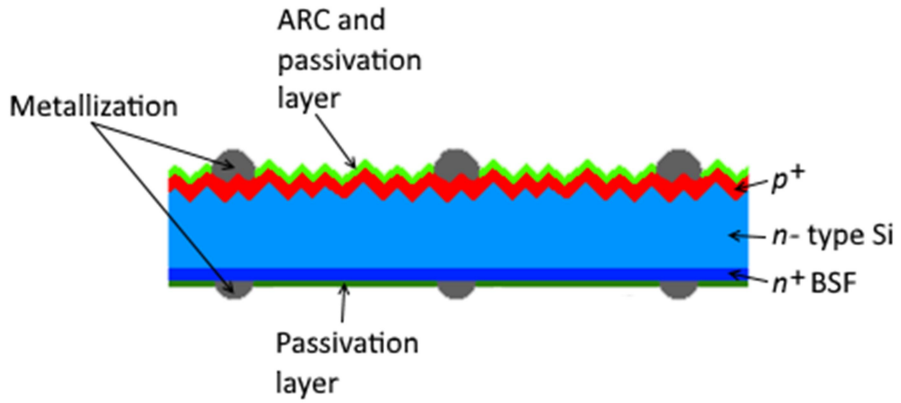

Fig. 3: Schematic cross-section of the *n*-PERT samples.

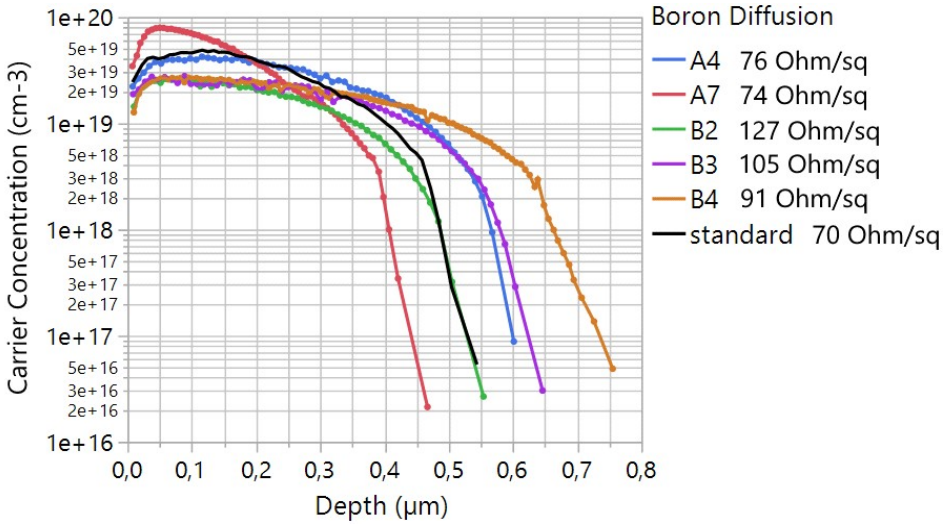

Fig. 4: Doping profiles of boron emitters measured by ECV at central position of the boat. Profiles B vary in the junction depth $d_{emitter}$ whereas profiles A vary in the peak concentration $N_{A\,peak}$ and junction depth.

From the QSSPC results (iV_{OC} and J_0, **Fig. 5**.) it is obvious that profiles with lower emitter surface concentration and higher sheet resistance give better passivation (higher iV_{OC} and lower J_0). The emitter depth has a less significant influence on the passivation quality on cells without metallization. The worst passivation quality of profiles A and the standard with higher surface concentration was caused by the increased recombination. This recombination came from

a stronger band-gap narrowing and thus a higher effective intrinsic charge carrier density.

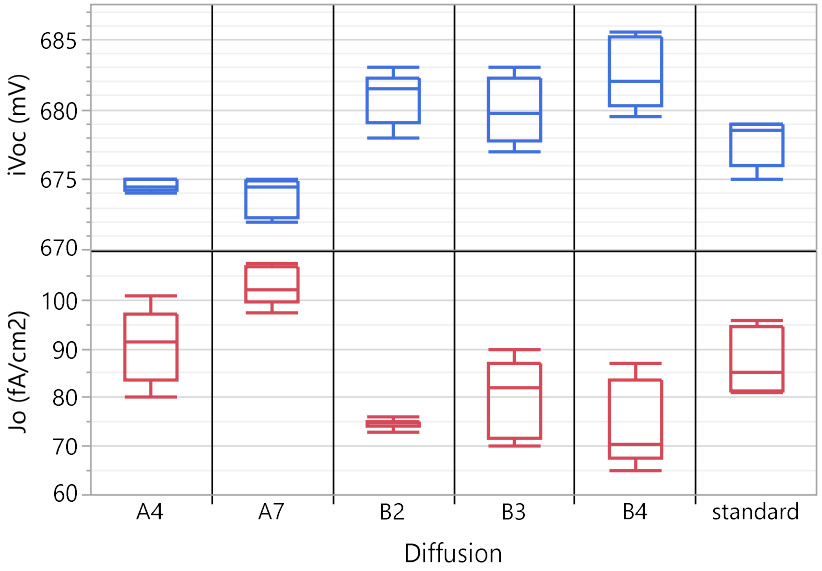

Fig. 5: iV_{OC} at 1 sun and J_0 of the cell precursors (before metallization). The J_0 was extracted at an injection level of $\Delta n = 3 \cdot 10^{15}$ cm^{-3}.

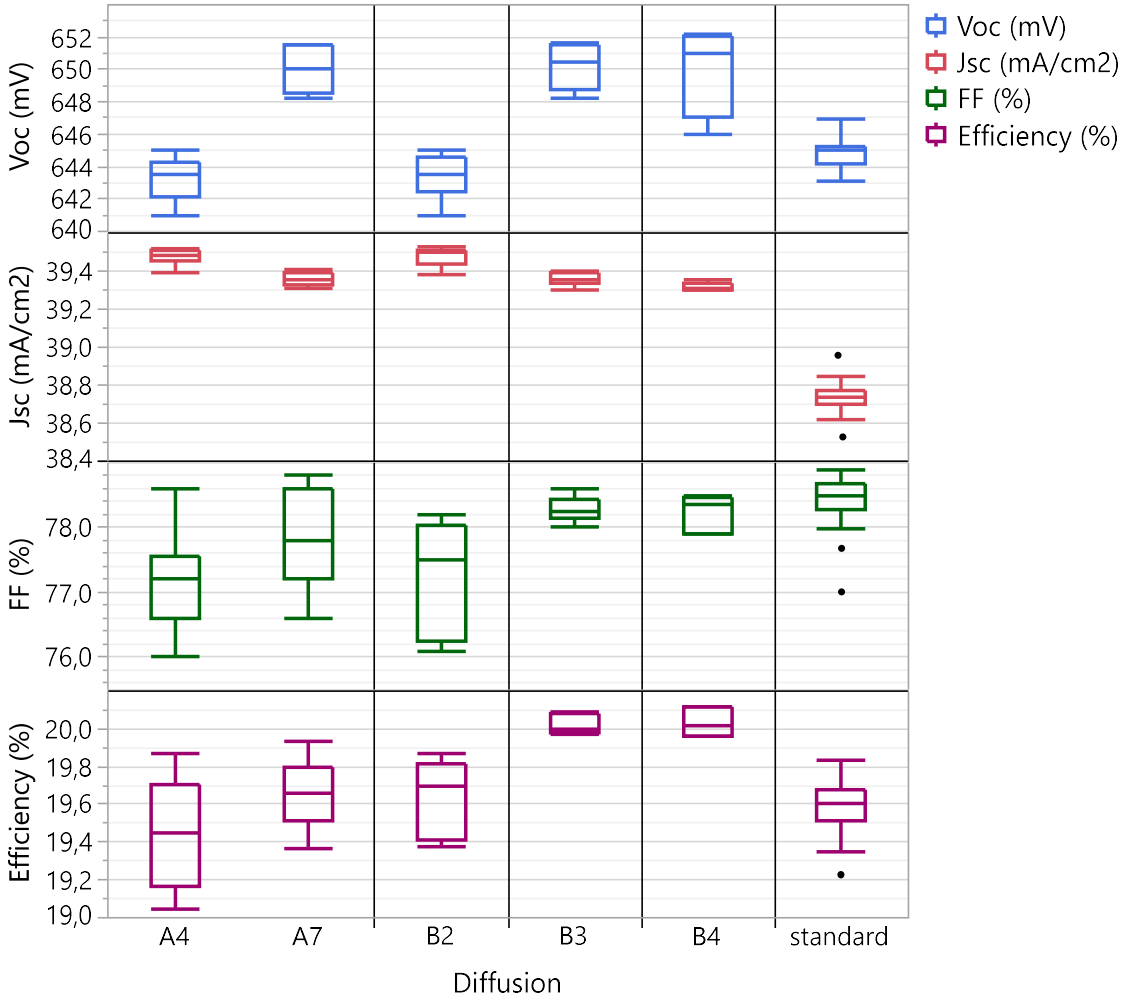

Fig. 6: Solar cell parameters obtained by IV measurement at 25 °C and under AM 1.5 spectrum with illumination intensity of 1000 W/m^2.

The results from IV measurement (**Fig. 6**) showed that, for screen printed and firing contacts, there is a trade-off between efficiency potential, demonstrated by the cell precursors and metalized cells. The best compromise is achieved for emitter profiles with low surface concentration (which gives better surface passivation) and emitter with higher depth (which prevent high contact recombination losses). The high value of J_{SC} and low V_{OC} in the case of samples with doping profile B2 is caused by insufficient emitter depth, which leads to higher recombination under the metal contacts.

This experiment led to optimization of emitter doping profile used at *n*-PERT solar cells with respect to following process steps – particularly metallization. As the new standard boron emitter profile, the profile B3 was set up, and used in following experiments. From the processability point of view it is necessary to mention that the maximum deviation of sheet resistance did not exceed 5 %, which is needed for good quality of metallization in further process steps.

3.1.2 Dry and wet oxidation at low pressure boron diffusion

An experiment using wet oxidation instead of dry oxidation was carried out together with the possibility of replacing atmospheric pressure diffusion with low pressure process. Four different low-pressure (LP) boron diffusion recipes were tested (**Tab. 1**). To compare the emitter quality between low-pressure and atmospheric-pressure (AP) process the samples with "standard" emitter were made. The wet or dry oxidation process took place between deposition and drive-in. The diffusion process for all LP recipes was the same except for the parameters of oxidation.

Tab. 1: The overview of used diffusion processes.

Diffusion		Type of Oxidation	Steamer		R_{Sh} [Ω/sq]
LP-1	Low-pressure	Dry	No	–	76
LP-2	Low-pressure	Wet	Yes	4 min	127
LP-3	Low-pressure	Wet	Yes	6 min	127
LP-4	Low-pressure	Dry	No	–	75
Standard	Atmospheric-pressure	Dry	No	–	70

The doping profiles are shown in **Fig. 7**. Because LP-2 and LP-3 differ from each other only slightly in the steam duration it was assumed that their emitters had the same properties. From the ECV measurement of samples LP-1 and LP-3 it is obvious that there were no significant changes in the emitter doping profile over the boat.

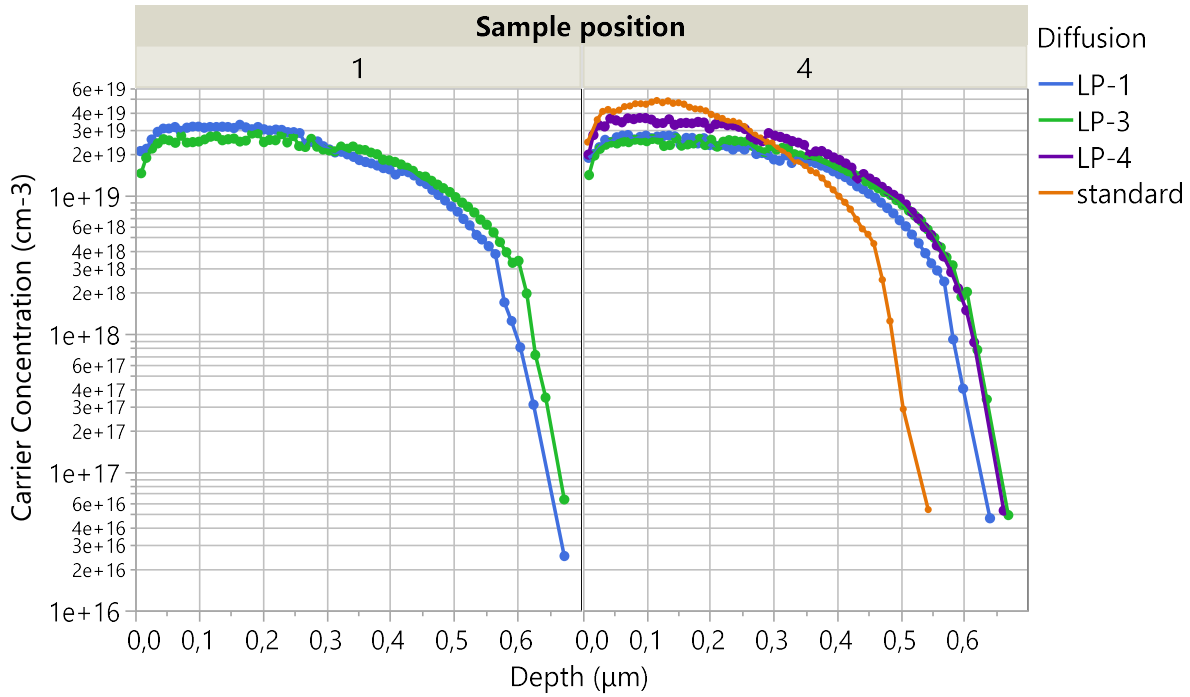

Fig. 7: The comparison of doping profiles for recipes LP-1 and LP-4 (dry oxidation), LP-3 (wet oxidation), and atmospheric pressure diffusion (standard). The position of wafer nearest to the gas inlet = 1, the position closest to the door = 5.

The R_{Sh} was measured using the four point measurement method (**Fig. 8**). Due to failure to achieve good homogeneity of the diffusion over the boat, only results for samples with R_{Sh} deviation of R_{Sh} below 5 % are mentioned further. The maximum deviation of R_{Sh} should not exceed 5 %, required for good quality of metallization.

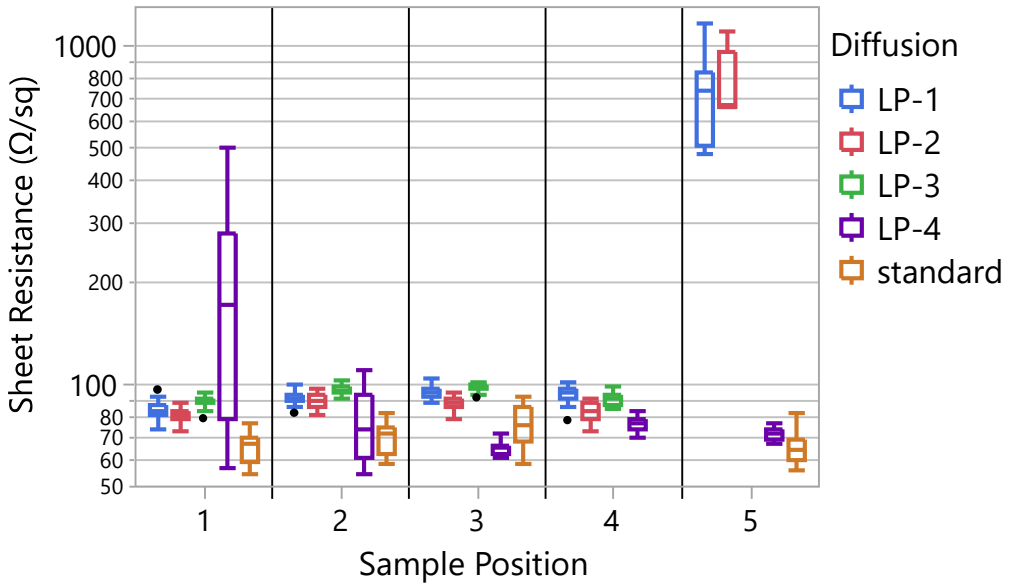

Fig. 8: The comparison of emitter R_{Sh} of all diffusion recipes. The position of wafer nearest to the gas inlet = 1, the position closest to the door = 5.

The thickness of BSG layer was measured by ellipsometry in five points on the front surface of the polished sample (**Fig. 9**). Owing to much better homogeneity of the BSG layer, the recipe LP-3 seemed to be a more suitable process.

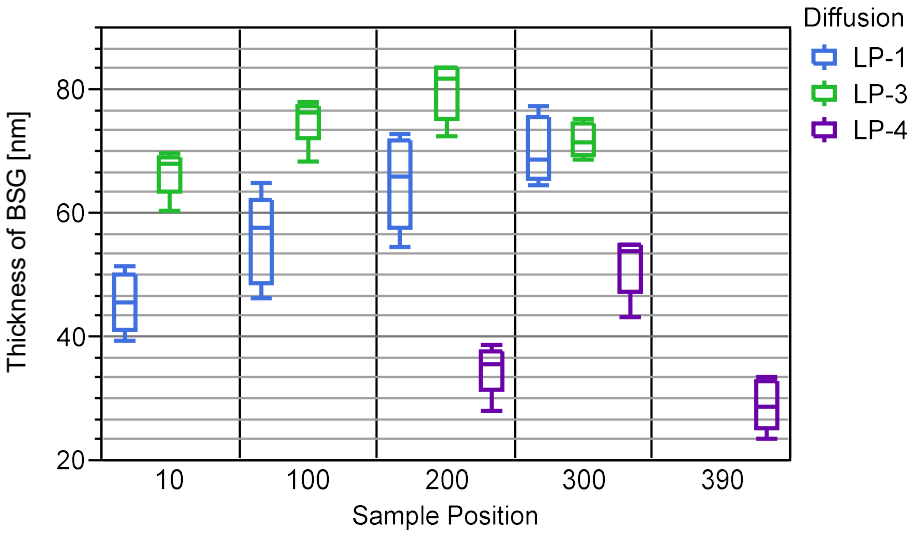

Fig. 9: The thickness of the BSG layer.

On the cell precursors the iV_{OC} and J_0 was measured before and after annealing using QSSPC to establish the influence of annealing on passivation quality (**Fig. 10**). The LP-4 samples were left out due to their high inhomogeneity near the gas inlet. The quality of the passivation layer before annealing was insufficient, low values of iV_{OC} and high values of J_0 indicated high recombination rate. The improvement of passivation after annealing came from releasing hydrogen during the hydrogenation process. All low pressure processes showed better passivation (lower J_0, higher iV_{OC}) in comparison with standard atmospheric pressure diffusion.

Fig. 10: iV_{OC} at 1 sun and J_0 of the cell precursors (before metallization) before and after annealing. The J_0 was extracted at an injection level of $\Delta n = 2 \cdot 10^{15}$ cm^{-3}.

Based on results from this experiment, it could be stated that dry oxidation process can be replaced with wet oxidation. Also, all low pressure processes showed better passivation (lower J_0, higher iV_{OC}) in comparison with standard atmospheric pressure diffusion and thus applicability for production of high efficiency *n*-type solar cells. Unfortunately, due to several technical problems with low pressure diffusion furnace there was no continuance in low-pressure diffusion processes.

3.2 PASSIVATION LAYER AND ANTIREFLECTIVE COATING

3.2.1 Minimal SiO_2 thickness and BSG etching rate

The possibility of use BSG as the intermediate layer between p^+ and SiN_X was investigated, because the passivation of the BSG layer alone is insufficient. The first part of this experiment was focused on measurement of etching BSG rate to control the thickness in the case of different diffusion processes. Three different boron emitters varying in doping profile were deposited to get different thickness of BSG layer with different content of boron in it (**Fig. 11**). The DEP profile (R_{Sh} > 200 Ω/sq) is not shown there, as this diffusion was done only to create very thin BSG layer. To see how the etching rate changed with the modification of BSG composition, an oxide with similar thickness was created on the *n*-type wafers using dry oxidation. The process of oxidation was the same as in the diffusion in the oxidation furnace. The BSG/oxide layer was made thinner by etching in bath containing 2% HCl and 2% HF solutions.

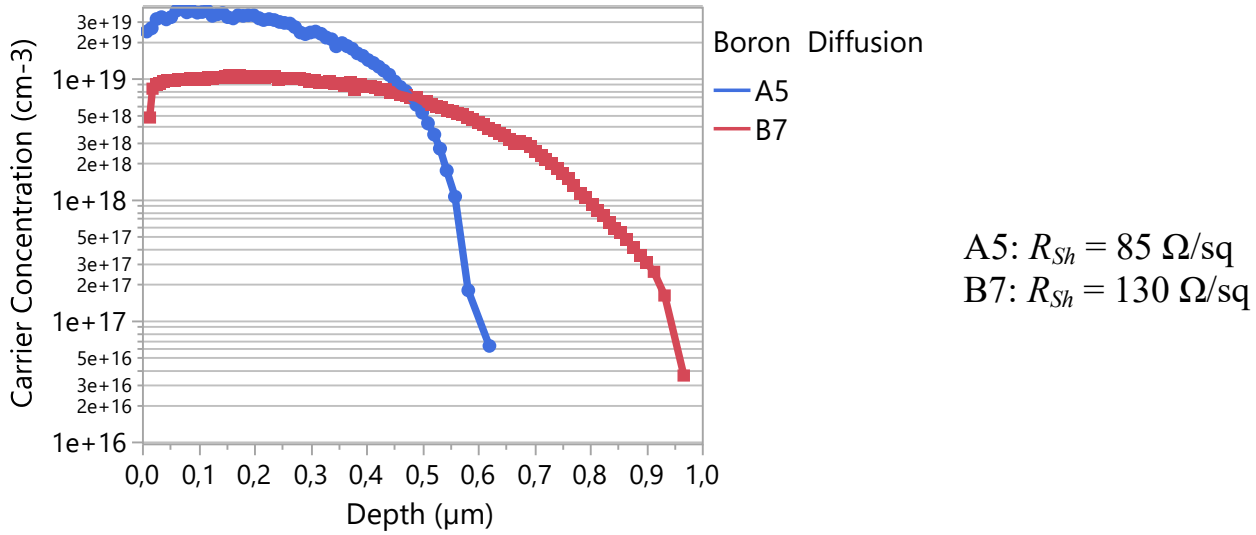

Fig. 11: Doping profiles A5 and B7 of boron emitter measured by ECV at central position of the boat.

The thickness of SiO_2 decreased during the etching almost constantly, the etching rate was ca. 0.2 nm/s **Fig. 12**. The etching rate in the case of BSG layers changed according to the boron content in it and thus was higher in the first third of its thickness. The etching process enables unification of the BSG thickness over the wafer. In case of layer BGS-DEP the etching rate was about 8 nm/sec.

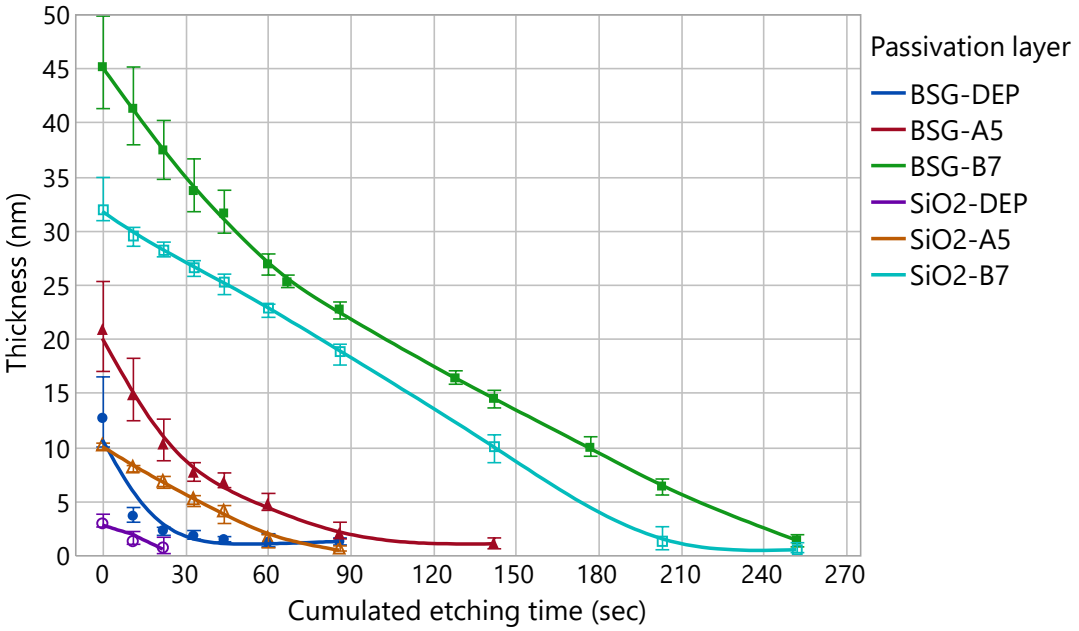

Fig. 12: The dependence of BSG/SiO_2 thickness on cumulated etching time.

In the second part of this experiment samples with symmetrical boron diffused test structure (**Fig. 13**) were created to find out the minimum SiO_2 thickness necessary for good passivation of boron layer. The samples were fabricated on 6-inch *n*-type monocrystalline Si wafers using standard industrial processes. Based on the QSSPC results (**Fig. 14**) the minimum thickness of 10 nm SiO_2 or BSG appears to be necessary to achieve good passivation of boron emitter. This value was used in the following experiments.

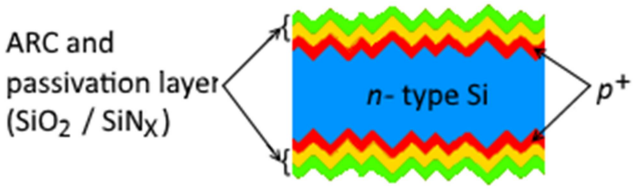

Fig. 13: Symmetrical $p^+/n/p^+$ test structures for QSSPC measurement.

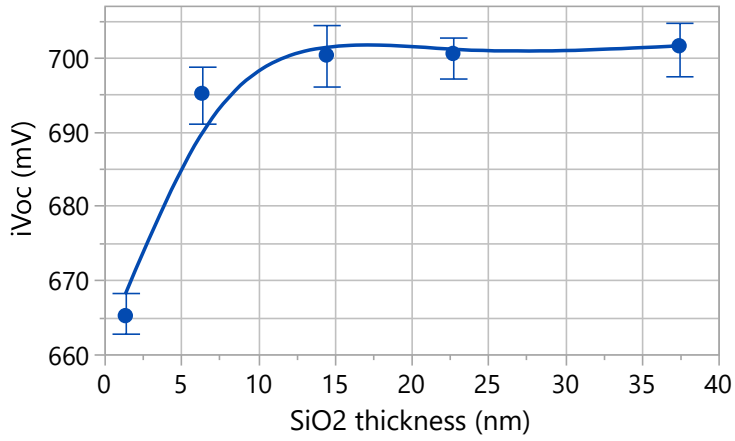

Fig. 14: iV_{OC} of symmetrical $p^+/n/p^+$ test structures with thermal SiO_2/SiN_X passivation stacks as a function of SiO_2 interfacial layer thickness

3.2.2 Boron emitter passivation by SiO_2 / PECVD SiN_X stack

The aim of this experiment was to study the passivation quality of BSG and PECVD-SiN_X stack at different boron diffusion. For this purpose two different structures were prepared (**Fig. 15**) – on the one hand an *n*-PERT cell with a homogeneous diffused front boron emitter and a phosphorus BSF; and on the other hand corona charge test structure. Both structures were fabricated on 6-inch *n*-type monocrystalline Si wafers using standard industrial processes.

All *n*-PERT cells were processed identically, with the exception of boron emitter passivation. For the boron emitter 5 different passivation stacks were investigated and compared (**Tab. 2**). The thickness and refractive index of SiO_2 or SiN_X layer were measured using ellipsometry on polished wafers on which these layers were created together with samples.

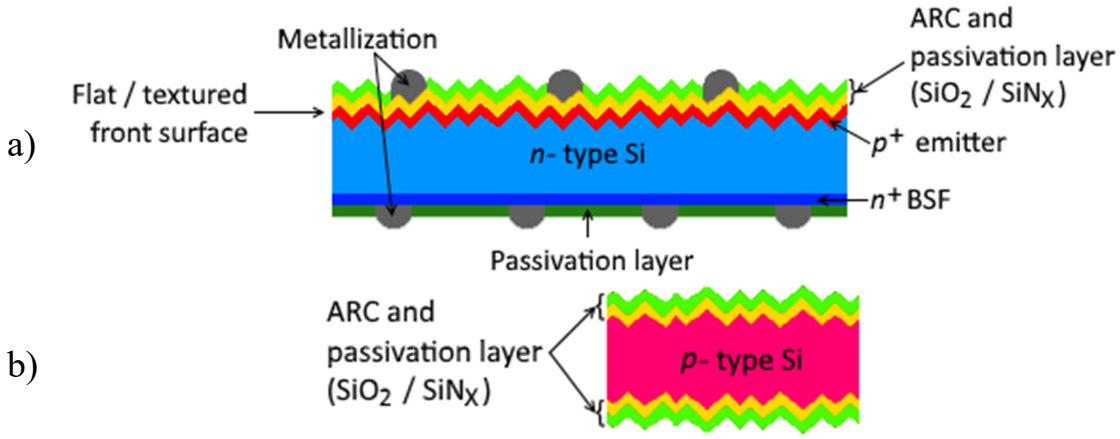

Fig. 15: Schematic cross-section of the investigated *n*-PERT cells (a) and test structure to corona charge measurement (b).

Tab. 2: The overview of investigated ARC layers. The thickness of layers was measured with ellipsometry on polished Si wafers which were deposited together with samples.

	G1	G2	G3	G4	G5
Emitter	p^+	p^+	p^+	p^+	p^+
1st layer	SiO_2 (10 nm)	SiO_2 (30 nm)	NAOS (1.5 nm)	SiO_2 (10 nm)	SiO_2 (10 nm)
2nd layer	SiN_X (n = 2.0)	SiN_X (n = 2.0)	SiN_X (n = 2.0)	SiN_X (n = 2.08)	SiN_X (n = 2.22)

On the cell precursors the iV_{OC} and J_0 (**Fig. 16**) were measured using QSSPC to establish how the PECVD SiN_X/SiO_2 stack influences the passivation quality. From iV_{OC} values it is obvious that the best passivation quality on the cell precursor level was achieved with G2.

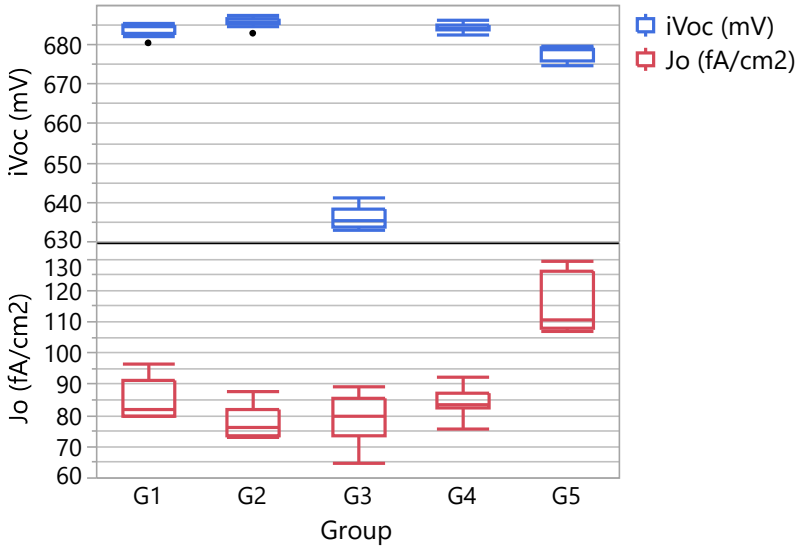

Fig. 16: iV_{OC} of the cell precursor (before metallization) obtained at 1 sun illumination and J0 extracted at an injection level of $\Delta n = 3 \cdot 10^{15}$ cm^{-3}.

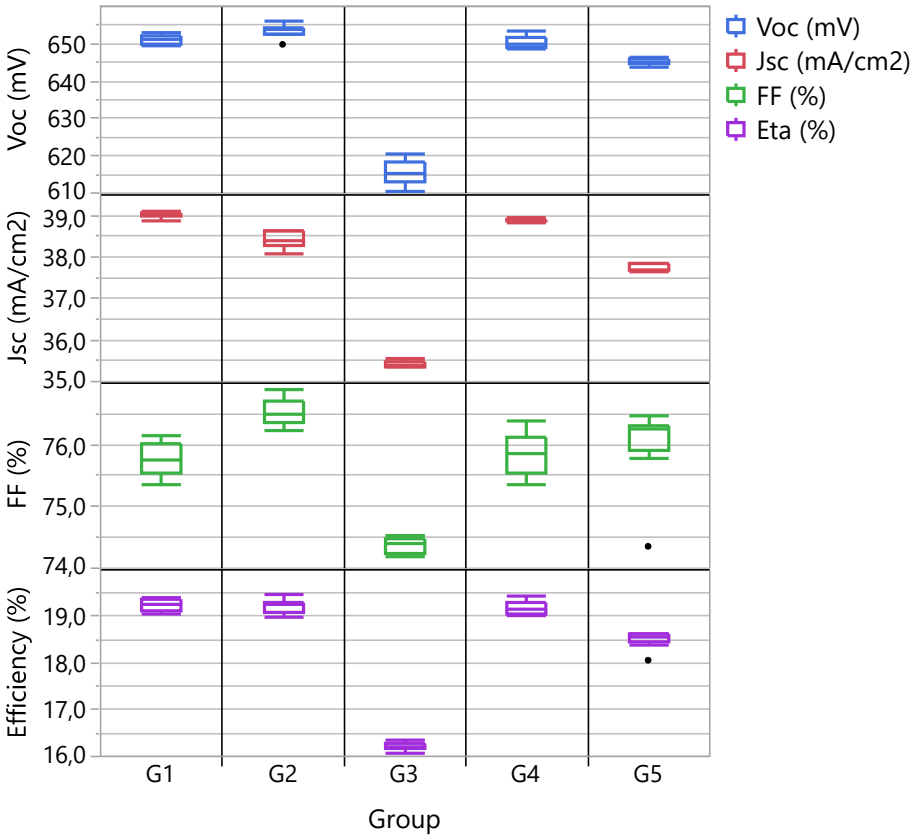

Fig. 17: V_{OC}, J_{SC} , *FF*, and efficiency values measured on metallized solar cells were obtained by IV measurement at 25 °C and under AM 1.5 spectrum with illumination intensity of 1000 W/m^2.

On finished solar cells the IV measurement (**Fig. 17**) was taken, and internal quantum efficiency (IQE), density of interface traps (D_{it}), and total fix interface charge (Q_{tot}) was measured (**Fig. 18**). The lower values of FF and efficiency were caused by not optimal grid structure. The passivation stacks G1 and G2 showed the best passivation quality, as there was no decrease at short wavelengths in contrast with the samples from G4, which had J_{SC} and V_{OC} values almost on the same level.

The absorption in SiN_X due to higher refractive index is not corrected in the IQE curve. So the reduction in IQE for G4 compared with G1 should be in SiN_X due to the additional absorption and not necessarily to the poorer passivation. It has to be said that the interface quality is very high (low D_{it}) although the interface charge of thermal oxide is very low.

The difference in IV results between G1 and G2 arises from different optical properties of passivation stack. The G2 gives slightly better passivation (higher V_{OC}) but the J_{SC} value was lowered due to optical losses caused by worse light coupling.

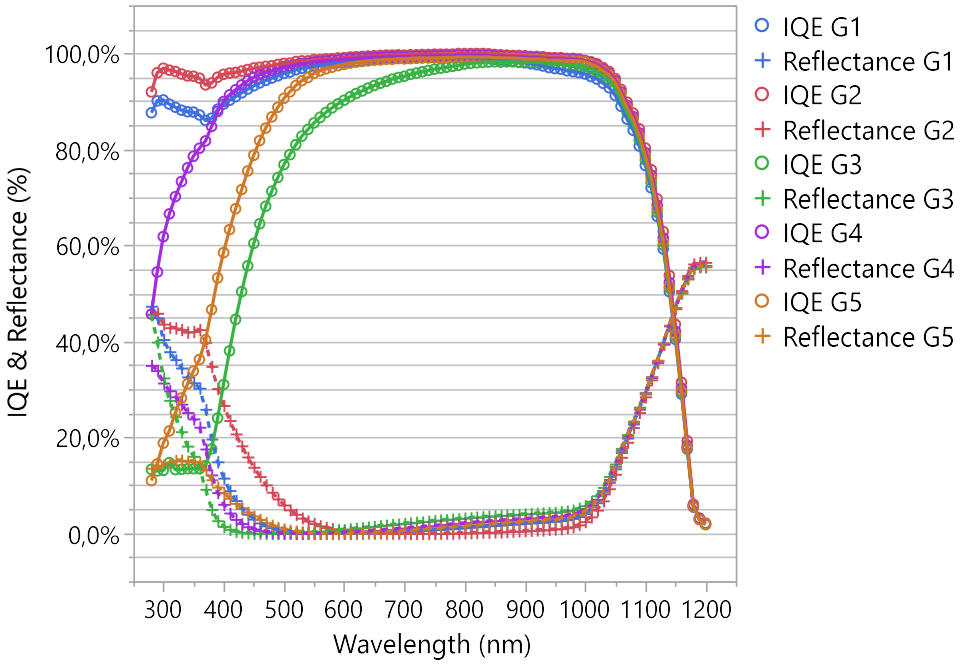

Fig. 18: Internal quantum efficiency (IQE) of the solar cells with different front boron emitter passivation stacks.

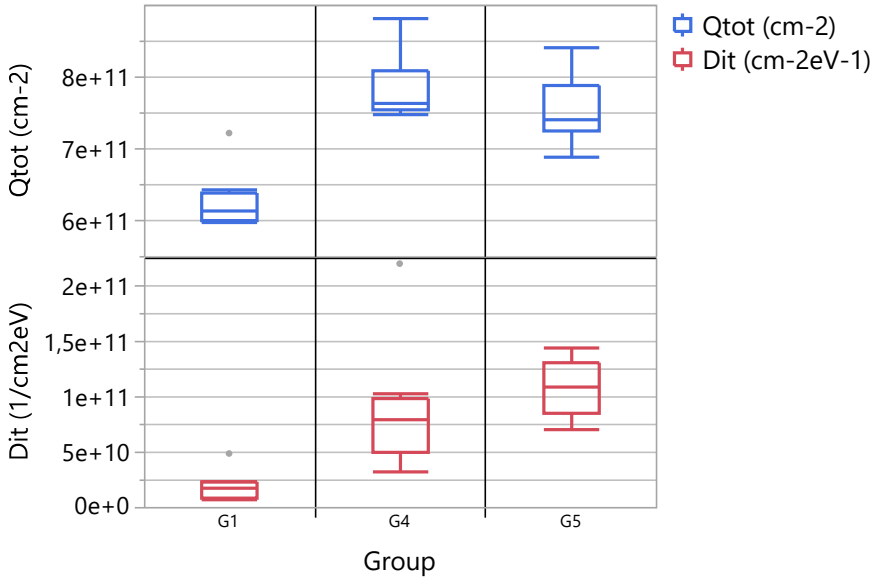

Fig. 19: Density of interface traps (D_{it}) and total fix interface charge (Q_{tot}) for different composition of SiN_X capping layer determined by corona charge measurements. The measurements were performed using Semilab PV2000 tool on un-diffused *p*-type c-Si wafers passivated by similar stack structures of G1, G4, and G5.

From the IQE results in the **Fig. 18** it is obvious that the passivation quality was worse in the case of SiN_X capping layers with higher refractive index despite the fact that these layers might be better for good passivation due to higher content of hydrogen. The reason is that the deposition SiN_X with higher refractive index also increased the density of interface states and positive interface charge (**Fig. 19**), which both had a negative effect on boron emitter passivation.

The results show that the optimum passivation in this case is achieved by a stack layer of a thermal SiO_2, with a thickness of at least 10 nm, and a SiN_X layer with a low refractive index. Using SiN_X layer with high refractive index ($n > 2.30$) would most probably required SiO_2 layer of thickness around 60 nm [9]. From the passivation results it is observed that the chemical SiO_2 deposited by NAOS method does not show good passivation quality. This could be caused by PECVD deposition of SiN_X, which could damage the thin SiO_2 layer. Also the chemical composition of SiN_X capping layer plays an important role for surface passivation. A more Si-rich SiN_X layer shows significant degradation in surface passivation of the stack due to the increase in the density of interface states and fixed positive charges at the interface.

3.2.3 Optimization of SiN_X thickness

The following experiment was done to investigate the impact of the rear silicon nitride thickness on the passivation quality and contact resistivity, and to determine the optimal thickness of passivation layer afterwards. For samples the 6'' monocrystalline Si phosphorus-doped *n*-type wafers were used. As the passivation layer on the rear side is composed from two layers, where one is with various thickness (**Fig. 20 a**), it was necessary to prepare samples dedicated only for measurement of varied SiN_X layer (**Fig. 20 b**).

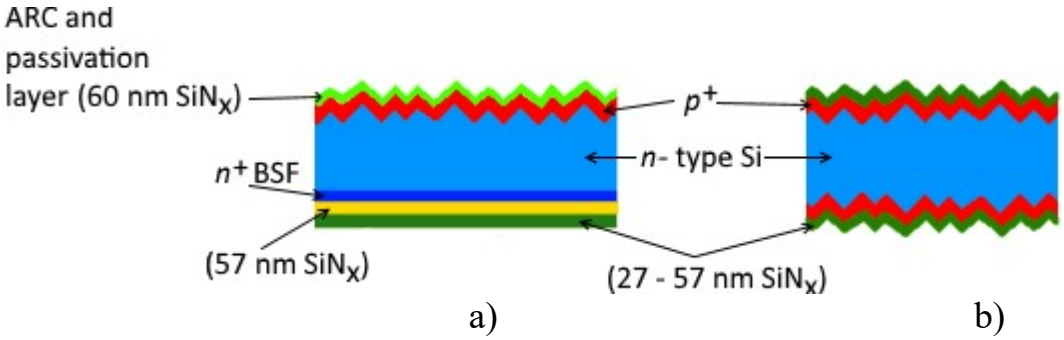

Fig. 20: a) The structure of cell precursor; b) Sample used for measurement of SiN_X thickness.

For the determination of thickness of SiN_X layer (d_{SiNX}) deposited on textured surface, a method based on the measurement of a reflectance spectrum of a wafer was used. The detector was inclined by 8° perpendicular to the sample. The dependence of reflection on the wavelength of incident light is shown in **Fig. 21**. The SiN_X thickness was calculated from the wavelength λ_{min} at the minimum of the reflectance curve according to:

$$d_{SiN_X} = \frac{\lambda_{min}}{4n_1}\sqrt{1 + \frac{{n_0}^2}{{n_1}^2}[\sin(90 - \theta)]^2} \qquad (1)$$

where n_0 was the refractive index of air ($n_0 = 1$), n_1 was the refractive index of SiN_X ($n_1 = 2.03$), and θ was the angle of incident beam ($\theta = 8°$) [10]. The resulting SiN_X thickness is given in **Tab. 3**. In the case of samples X and Y the SiN_X thickness was evaluated from extrapolation based on deposition time $t_{deposition}$.

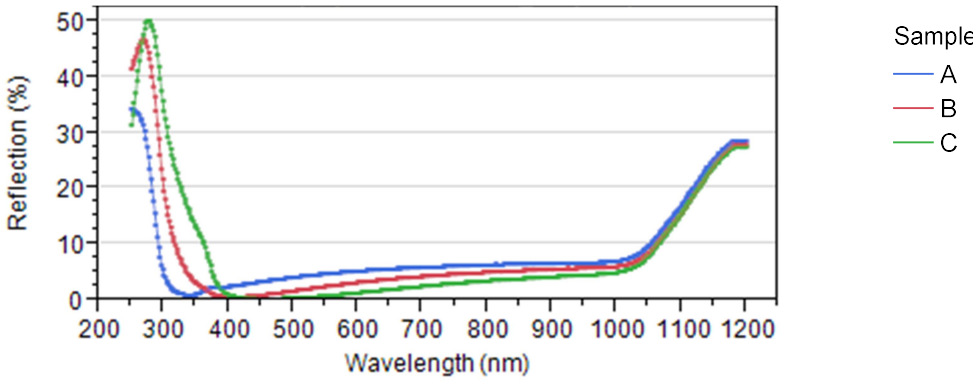

Fig. 21: The reflectance of samples with $t_{deposition}$ 480 s, 580 s, and 680 s.

Tab. 3: Calculated of SiN_X thickness for samples on the rear side.

Sample	$t_{deposition}$ [s]	λ_{min} [nm]	d_{SiNX} [nm]
X	280	-	27.2
Y	380	-	34.8
A	480	341	42.1
B	580	406	50.1
C	680	462	57.0

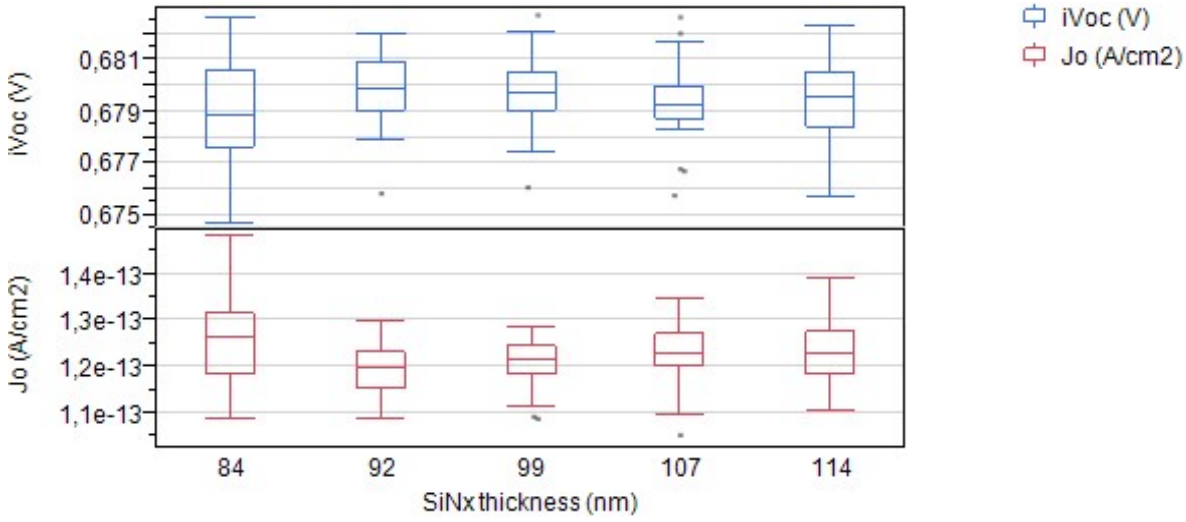

Fig. 22: iV_{OC} at 1 sun and J_0 of the cell precursors. The J_0 was extracted at an injection level of $\Delta n = 2 \cdot 10^{15}$ cm^{-3}.

It is obvious that the best passivation quality (high iV_{OC} and low J_0 measured by QSSPC on the cell precursors) is achieved in the SiN_X layer with average thickness of 92 nm and 99 nm (**Fig. 22**).

The screen-printed silver finger grid at the front and the rear side was dried and subsequently co-fired in an infrared belt furnace. The three used temperature profiles differed from each other in the maximum temperature to evaluate the influence of firing metallization on contact resistivity. The peak temperature was set to 780 °C, 795 °C, and 815°C. The contact resistivity (ρ_C), characterizing the interfacial perfection between a conducting material and an underlying semiconductor, was detected by the Transmission Line Model (TLM) method (**Fig. 23**).

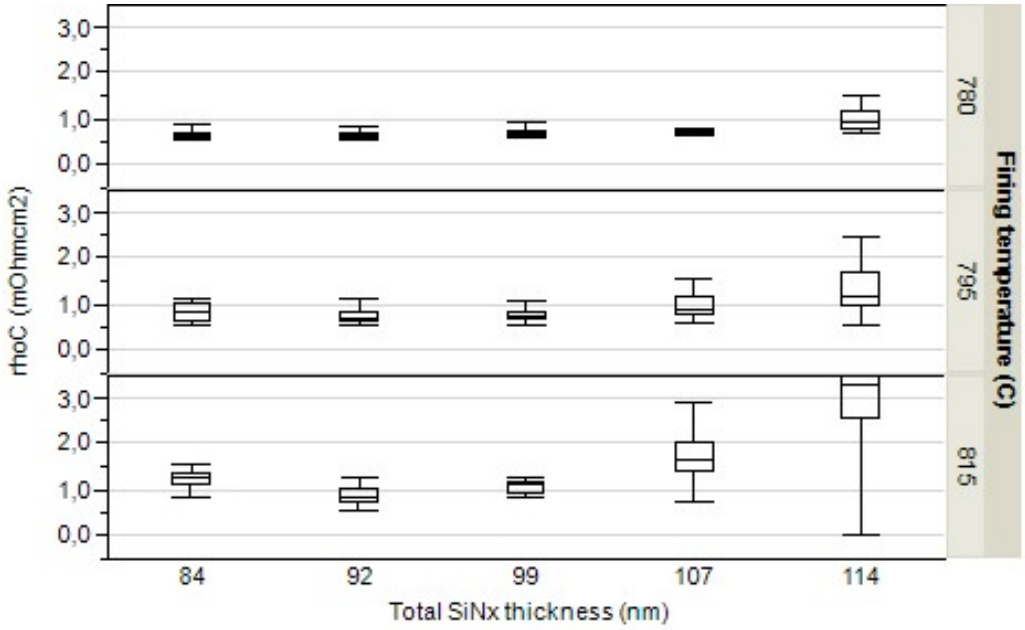

Fig. 23: The influence of SiNX thickness and peak firing temperature on resulting ρ_C.

The results of this experiment show that the value of contact resistivity depends mainly on the firing profile (in this case v_{peak}) and much less on SiN_X thickness, which had big impact on passivation quality, as the best passivation quality (high iV_{OC}, and low J_0) results in SiN_X layer with average thickness $d_{SiNX} = 92$ nm. The lowest contact resistivity was achieved for combination of low firing temperature and total SiN_X thickness of 84 nm. Based on this experiment the peak firing temperature of 780 °C was used in solar cell production.

3.3 PREVENTION OF PID AT THE CELL LEVEL

This work is focused on the influence of different composition of ARC layer on Potential Induced Degradation (PID) effect at *n*-PERT cell concept [11] [12] [13]. A schematic cross-section of the studied solar cells is presented in **Fig. 24**. For the experiment, 6-inch *n*-type mono-Si substrates were used. Half of the samples had textured front side, the rest of them had flat front side. In this experiment, 8 different compositions of ARC layer were tested (**Tab. 4**). The thickness of layers was measured with ellipsometry on flat silicon wafers, which were deposited together with the samples. Full-size 3 busbar single cell modules were fabricated using solar

textured cover glass, ethylene-vinyl acetate copolymer (EVA-S88) for the encapsulation, and standard transparent back sheet material (**Fig. 25**).

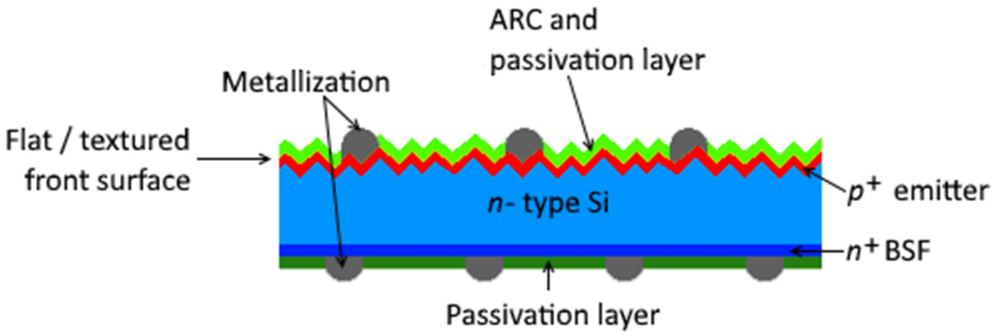

Fig. 24: Schematic cross-section of the investigated *n*-PERT cells.

Tab. 4: The overview of investigated ARC layers.

	G1	G2	G3	G4	G5	G6	G7
Emitter	p^+	p^+	p^+	p^+	p^+	p^+	p^+
1st layer	SiO_2 (10 nm)	SiO_2 (30 nm)	NAOS (1.5 nm)	SiO_2 (10 nm)	SiO_2 (10 nm)	SiO_2 (10 nm)	NAOS (1.5 nm)
2nd layer	SiN_X (n = 2.0)	SiN_X (n = 2.0)	SiN_X (n = 2.0)	SiN_X (n = 2.08)	SiN_X (n = 2.22)	SiN_X (n = 2.22)	SiO_2 (20 nm)
3rd layer						SiO_2 (100 nm)	SiN_X (n = 2.0)

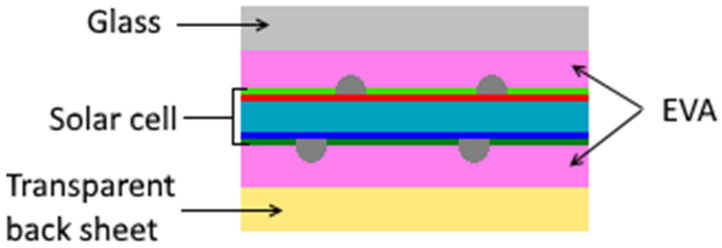

Fig. 25: Schematic cross-section of the investigated module.

The PID tests were performed according to technical specification IEC 62804-1 [14]. The modules were characterized before and after PID testing by electroluminescence (EL), IV measurements, reflection and IQE. Measurements were taken on both sides of the module to establish whether the degradation was occurring on the front side, rear side or both.

The IV measurements of modules were done to determine changes in J_{SC}, V_{OC}, efficiency, *FF,* and pseudo-fill factor *pFF*. The origin of the power drop in the PID effect is a decrease of J_{SC} and V_{OC}. Fill factor and pseudo fill factor stay nearly constant for all samples, which indicates that PID does not cause cell shunting. The severe J_{SC} degradation measured in experiments suggests an additional effect, e.g. a decrease of the diffusion length in the emitter due to contamination by in-diffused ions. More detailed characterization is needed to identify the root cause of this degradation mechanism.

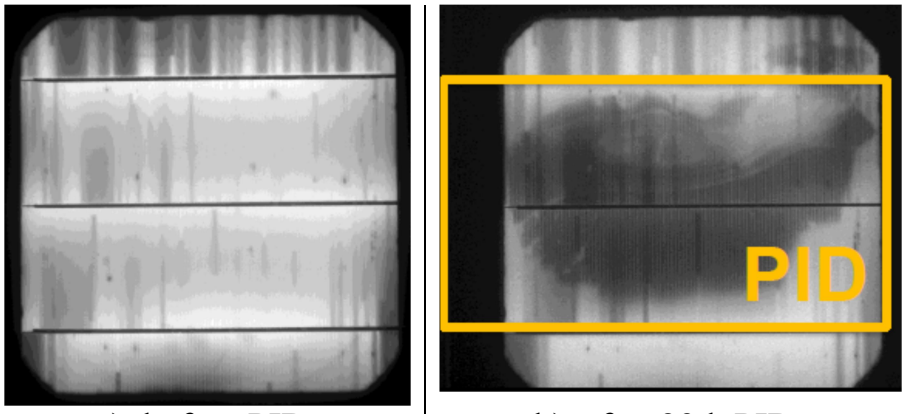

Fig. 26: EL picture of samples G2 with textured surface in the initial state (a) and after 23 h degradation (b).

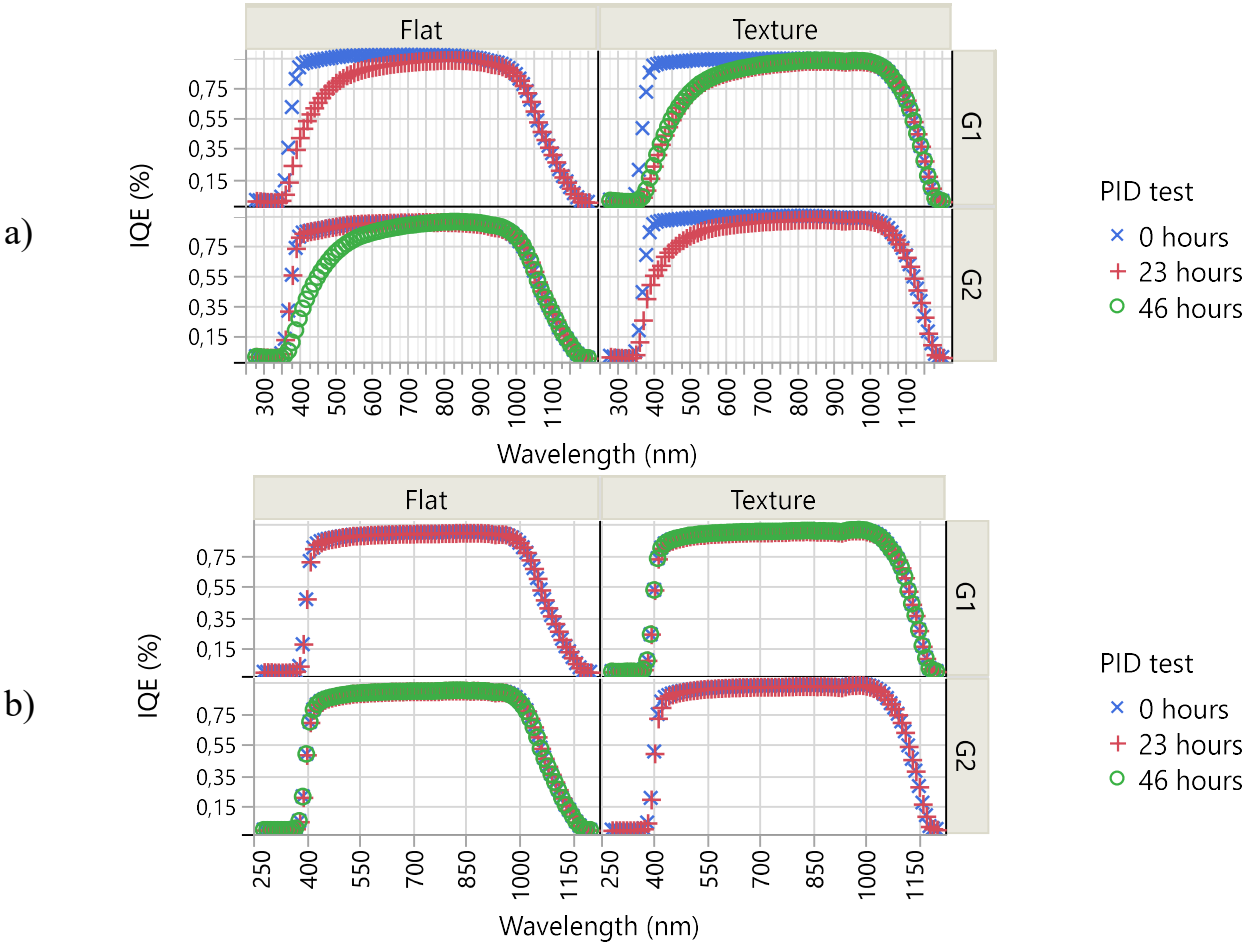

Fig. 27: Examples of the internal quantum efficiency IQE measured on the front (a) / rear (b) side of the solar cell where this side was textured or flat.

The EL measurements were taken to obtain the impression of the behaviour of solar cells under PID stress. **Fig. 26** shows examples of EL images for the mini-module before and after the PID test. The EL reveals localized defects of the module after PID state where lower signal means that the non-radiative recombination in the solar cell has increased. This is another indication that the power drop is caused by a loss of front surface passivation.

Comparison of the IQE (**Fig. 27**) of the front versus rear side indicates that the degradation process is related to the degradation of the front side of solar cell. Due to damage of some modules it was not possible to measure IQE after 46 hours at all samples. The type of texturization has no significant influence on the degradation. The decrease in IQE could be caused by the increase of the value of the front surface recombination velocity, which leads to the decrease of spectral response in the short-wavelength region ($\lambda < 500$ nm). Short-wavelength photons are absorbed in the heavily doped part of the emitter. Therefore the change of IQE spectrum could be caused by the enhanced front surface recombination.

3.4 METALLIZATION OF BORON EMITTER

3.4.1 In-situ resistance measurement

The influence of sintering conditions on the formation process of screen printed contacts on passivated boron emitters was measured by resistance R_C changes during firing thanks to in-situ contact resistance measurement method. For this experiment, 6-inch *n*-type mono-Si substrates were used (**Fig. 28**). The testing structure was created by 4 mm × 1 mm screen printed spots at 50 mm distance using pure Ag paste (A) and AgAl paste (B). The firing was done with a rapid thermal processing (RTP) furnace modified for in-situ resistance measurements (**Fig. 29**), where the change of resistance was measured simultaneously with the temperature by four point method.

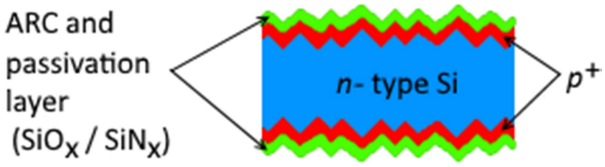

Fig. 28: Schematic cross-section of the symmetric samples.

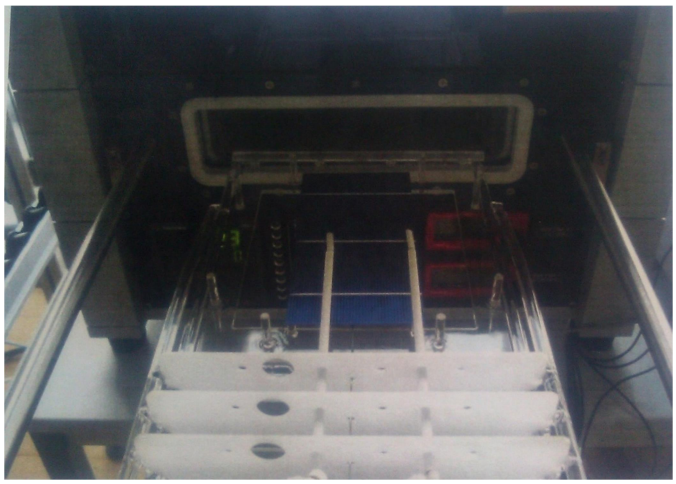

Fig. 29: RTP furnace modified for in-situ resistance measurement.

Two different temperature profiles labelled were used (see **Fig. 30**). In case of Profile 480, the composition of the process gas was changed using the O_2 concentration between 21 % and 0 % keeping the total gas flow constant. In the case of Profile 400, only the measurements with 21 % O_2 were taken.

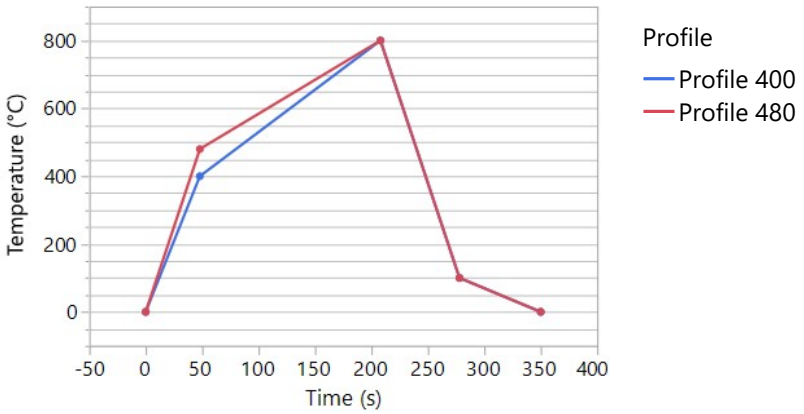

Fig. 30: Used temperature profiles labelled Profile 480 and Profile 400.

The resistance changes for Profile 480 are shown in **Fig. 31**. It is obvious that at the beginning there was no conductive connection between testing spots. They were separated from the substrate by deposited antireflection and passivation layer. The burning through the passivation layer at temperature ϑ_{BT} is indicated by the first conductive state. From graphs it is evident, that with the reduction of O_2 concentration, the first insulating state became shorter and the temperature ϑ_{BT} decreased. The fluctuations between 750 °C and 800 °C were most probably caused by rearrangement of silver particles in the liquid glass phase.

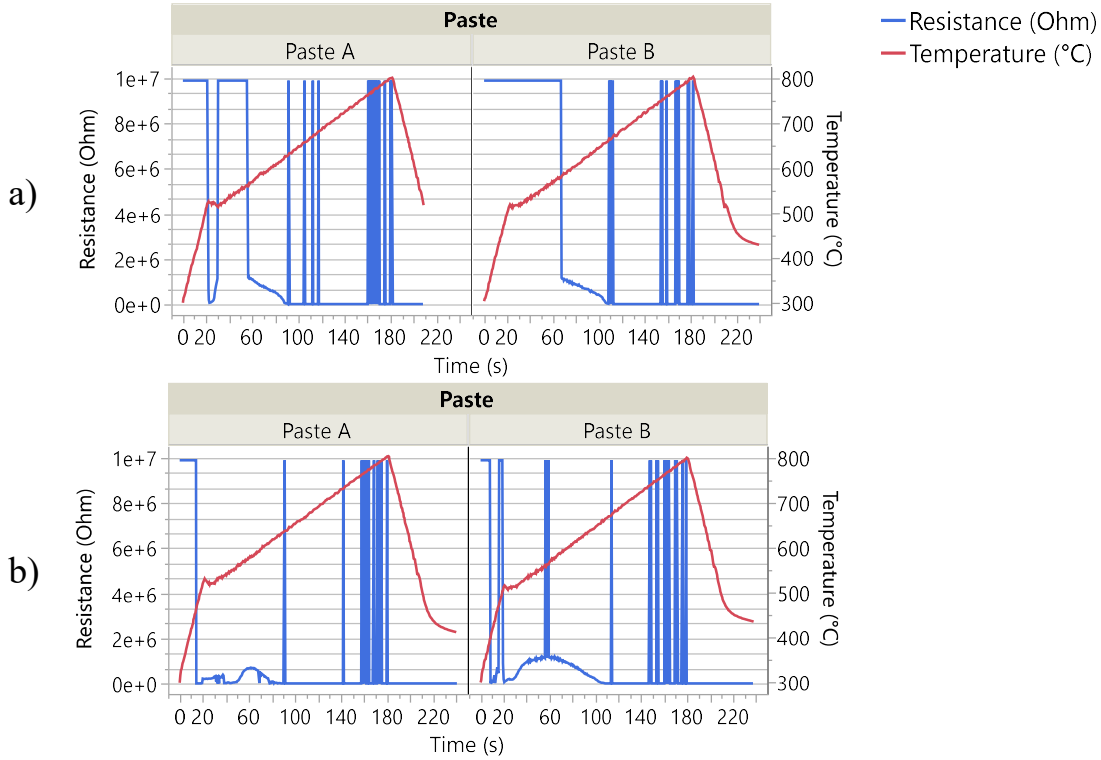

Fig. 31: Examples of in-situ resistance measurements using Profile 480 with: a) 21 % of O_2; b) 0 % of O_2 in process atmosphere.

From **Fig. 31 a)** and **Fig. 32** it is obvious, that the time necessary to burning through the ARC and passivation layer became shorter in both cases. The temperature ϑ_{BT} decreased from 525°C to 480 °C for paste A, and from 665°C to

368 °C for paste B. Up to 630°C, the paste B became conductive and no further insulating state was found.

It is clear that in-situ resistance measurements proved to give insight in the kinetics of contact formation and showed differences in the contact formation process for different O_2 concentrations and temperature profiles. The temperature required for burning through the dielectric layer could be determined from the resistance profile.

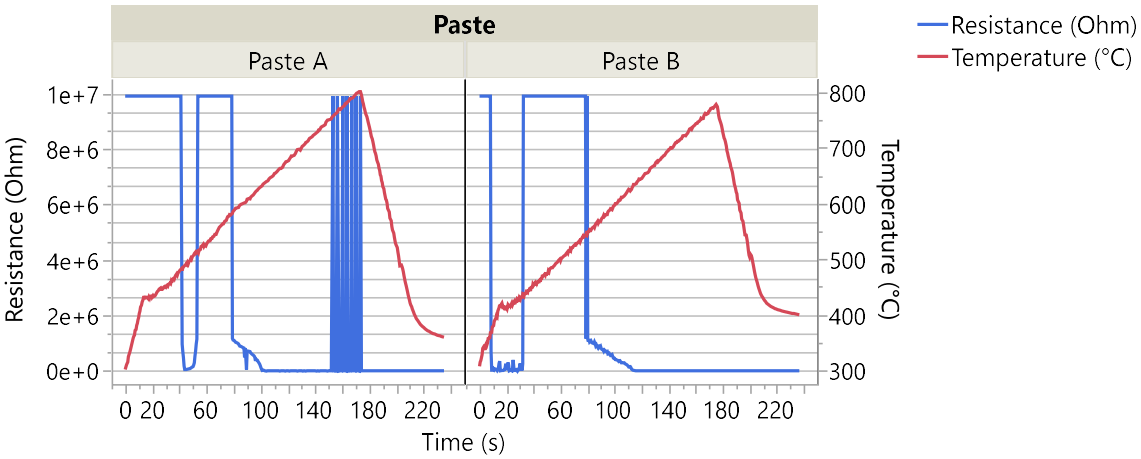

Fig. 32: In situ resistance measurement using Profile 400 with 21 % of O_2 in atmosphere.

3.4.2 Metallization induced losses

The following experiment focused on metallization induced losses was done to find the balance between doping profile and composition of metallization paste. The saturation current densities $J_{0\text{-}met}$ losses were determined for pure Ag paste and AgAl paste to establish the possibility of printing metallization by pure silver paste on boron emitter. The experiment was done using *n*-PERT solar cells (**Fig. 3**) with homogeneous boron diffused emitter and phosphorus diffused BSF on *n*-type mono-Si wafers. The wafers were processed using standard industrial processes. For this study, five different boron emitters (**Fig. 4**) were realized with different doping profile, and resulting sheet resistance. To determine the saturation current densities $J_{0\,E\,pass}$ of the passivated boron emitter, symmetric life-time samples (**Fig. 28**) were fabricated in parallel with the solar cells.

The finger grid at the front side and the rear side was screen printed using a commercial firing-through AgAl paste (only front side) or a pure Ag paste (both sides). The metallization fraction was variable on the front side to extract the $J_{0\text{-}met}$ under the metal contact for each combination of emitter/paste (**Tab. 5**) while it was kept constant on the rear side of the solar cell.

Tab. 5: Overview of used metallization fraction F_M.

Paste	Metallization fraction F_M [%]		
AgAl	4.43	12.29	20.16
Ag	4.51	12.52	20.53

The metalized solar cells were investigated by IV measurements to determine the values of J_{SC} and V_{OC}. The solar cells were measured under AM 1.5 spectrum with illumination intensity of 1000 W/m^2 and temperature of 25 °C. The metallization induced recombination losses for different boron emitters were calculated from IVdata using method described in [15]. The dependency of $J_{0\text{-}met}$ on the junction depth $d_{emitter}$ is shown in **Fig. 33**, dependency on the peak surface carrier concentration $N_{A\ peak}$ is in **Fig. 34**.

From the results in **Fig. 33** and **Fig. 34** it is obvious that almost similar $J_{0\text{-}met}$ values were obtained when boron emitters were contacted by AgAl firing-through paste (industrial state-of-the-art) or pure Ag paste. Deeper junction ($d_{emitter}$ more than 0.6 µm) led to the lower recombination underneath the metal contacts. The lowest $J_{0\text{-}met}$ values were obtained for doping profile A7 with high surface carrier concentration N_A, and for doping profile B4 with high emitter depth. However, the results A7 were in a strong contrast with the results described in chapter 3.1.1, where low surface carrier concentration was the optimum. Based on these results, the possibility of metallization printing by pure silver paste on both sides was included to the standard process.

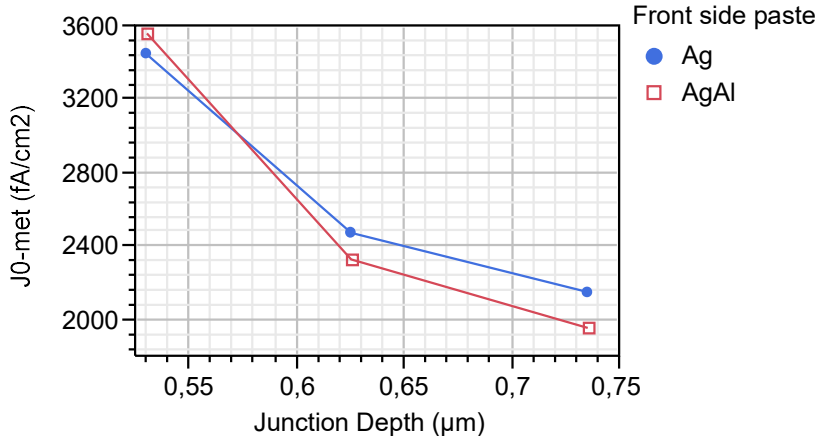

Fig. 33: The dependency of metallization induced losses $J_{0\text{-}met}$ on the junction depth $d_{emitter}$.

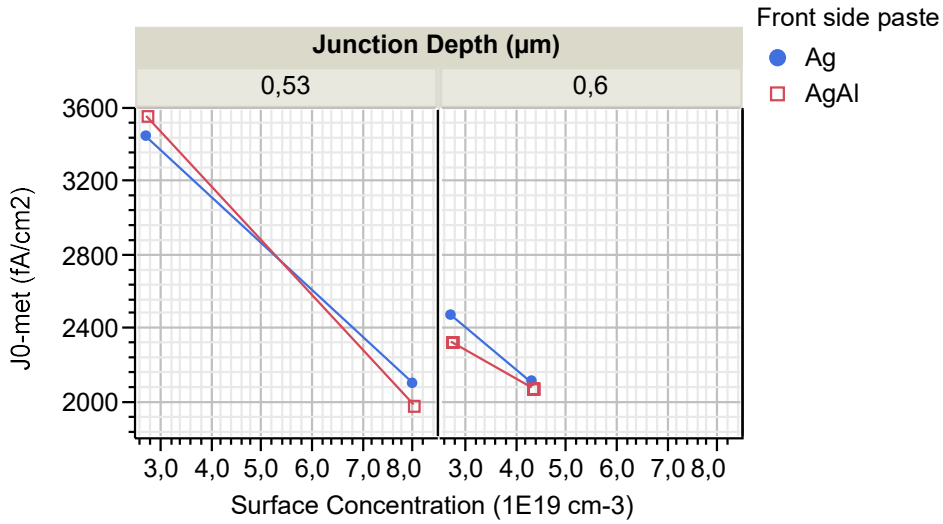

Fig. 34: The dependency of metallization induced losses $J_{0\text{-}met}$ on the peak surface carrier concentration $N_{A\ peak}$ for two different junction depths $d_{emitter}$.

3.4.3 Metallization variation

A strong loss in V_{OC} for solar cells using screen-printed metallization has been observed when comparing the iV_{OC} of passivated cell precursors with the actual V_{OC} of the finished solar cells [16] [17]. This could result from the high emitter surface recombination at the contacts, which can be overcome by decrease of the area metallized by firing-through paste. On that account, the following experiment was done. The *n*-PERT solar cells (**Fig. 3**) with homogeneous boron diffused emitter (standard profile, $R_{Sh} = 70\ \Omega$/sq) and phosphorus diffused BSF on *n*-type monocrystalline Si wafers were made using standard industrial processes. Six different metallization schemes were realized (**Tab. 6**, **Fig. 35**).

Tab. 6: Overview of used finger width and metallization steps. (BB = busbars).

Group	1st print paste A	2nd print paste B	2nd print paste C	Distance between fingers
G1	50 µm	only BB		1.719 mm
G2	pads 20 µm	38 µm + BB		1.719 mm
G3	20 µm	38 µm + BB		1.719 mm
G4	20 µm	38 µm + BB		1.719 mm
G5	38 µm + BB			1.719 mm
G6	20 µm		38 µm + BB	1.719 mm

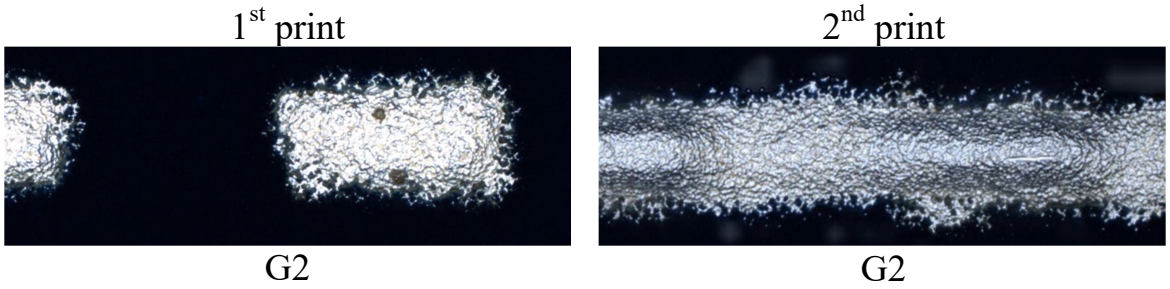

Fig. 35: An example of printed patterns.

After firing metallization, the IV measurements (**Fig. 37**) were taken. From comparison between G1 and G5 follows small V_{OC} gain if the busbars are printed separately. This phenomenon was investigated separately in the experiment described in the following chapter (3.4.4). The J_{SC} values for all groups except G1 and G6 are comparable. The lower value in case of G1 is mainly caused by shading. The lower J_{SC} of G6 probably results from the existence of oxide layer created during firing between firing through and non-firing pastes. The best efficiency and FF were achieved by samples from G3. All other groups performed worse. From PL images (**Fig. 36**) it is clear that the highest V_{OC} was achieved in the case of G2 and G4 samples.

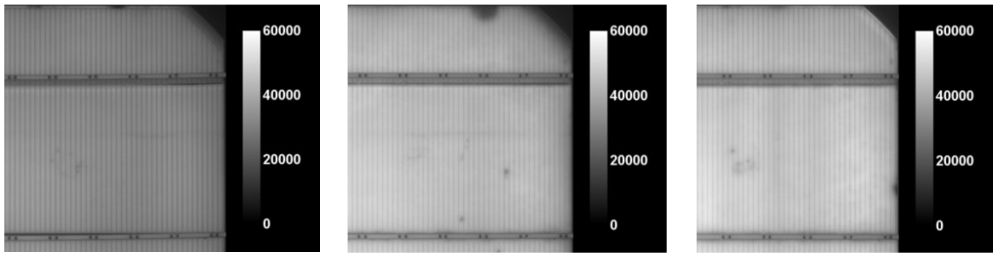

Fig. 36: Examples of solar cells PL images with different metallization. The light intensity correlates with V_{OC}.

The line resistivity R_L was measured using four point probe method. High R_L values for group G6 were caused by low conductivity of the non-firing paste. Other three double printed groups (G2 – G4) show comparable line resistivity results. The group G1 has the lowest R_L, owing to the line width of 50 µm instead of 38 µm (in total) used in the rest of the samples. Difference between G3 and G4 results from lower amount of paste printed on G4 samples.

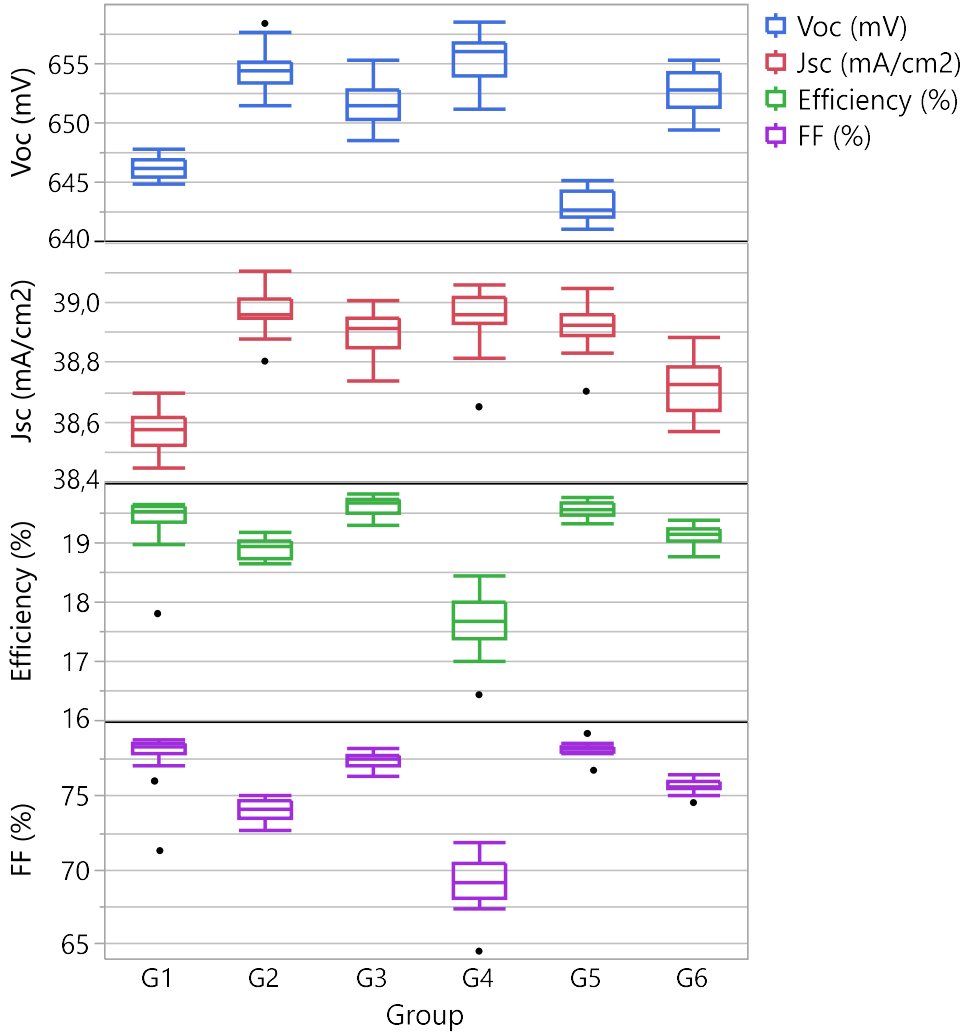

Fig. 37: Solar cell parameters obtained by IV measurement at 25 °C and under AM 1.5 spectrum with illumination intensity of 1000 W/m^2.

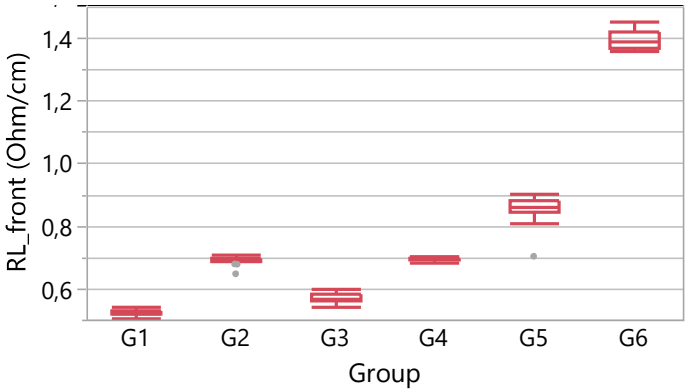

Fig. 38: Line resistivity of front side metallization.

3.4.4 Wafer orientation during firing

In this work the „grey finger“ phenomenon [18] was studied on boron doped surfaces. The orientation of the wafer on the belt and the presence of the busbars during firing influence the contact resistivity. By measuring the ρ_C, the impact of short-circuit effect was quantified. The samples (**Fig. 3**) were fabricated using 6-inch n-type mono-Cz Si wafers using standard industrial processes.

After annealing, but before the metallization step, the QSSPC measurement was taken to obtain the iV_{OC} and J_0 values. There were no significant differences between groups in the iV_{OC} and J_0 values thus it can be expected that resulting differences would come from firing process.

A commercially available firing-through pure Ag paste or AgAl paste were applied for metallization, where two screens were used. The first screen had a conventional H-pattern with 3 busbars (**Fig. 39** a). To mitigate the so called “short-circuit” effect, the H-pattern layout was modified so that only fingers were printed and fired (**Fig. 39** b, c). The metallization was dried and subsequently fired in an infrared-heating belt furnace. To establish the influence of wafer orientation during firing, the wafers were positioned with finger perpendicular (**Fig. 39** a, c) or parallel to the belt (**Fig. 39** b). On the cells where only finger were fired, the busbars were created afterwards by a non-firing paste which was only dried.

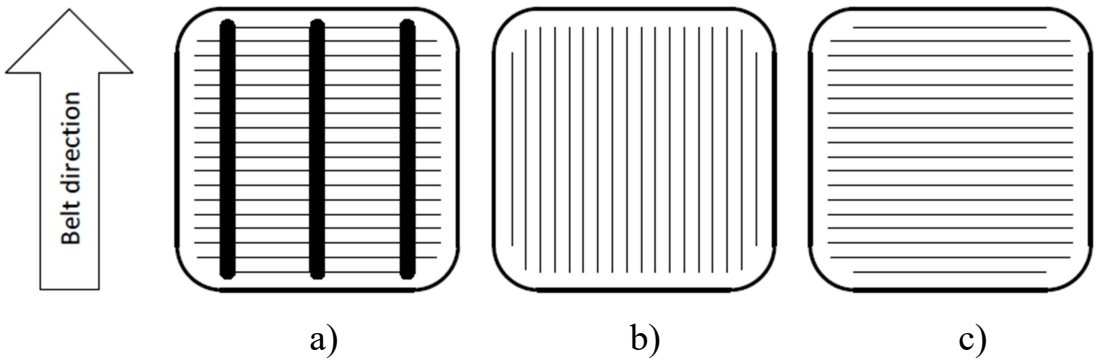

Fig. 39: Simplified screen layout that includes fingers and 3 busbars, and layout that excludes the busbars to mitigate the short-circuit effect.

After firing metallization, the IV measurement was taken and from the results in **Fig. 40** it is clear that the worst combination of printing and firing was printing of Ag paste with busbars. In the case of the cells fired without busbars the orientation didn't play important role.

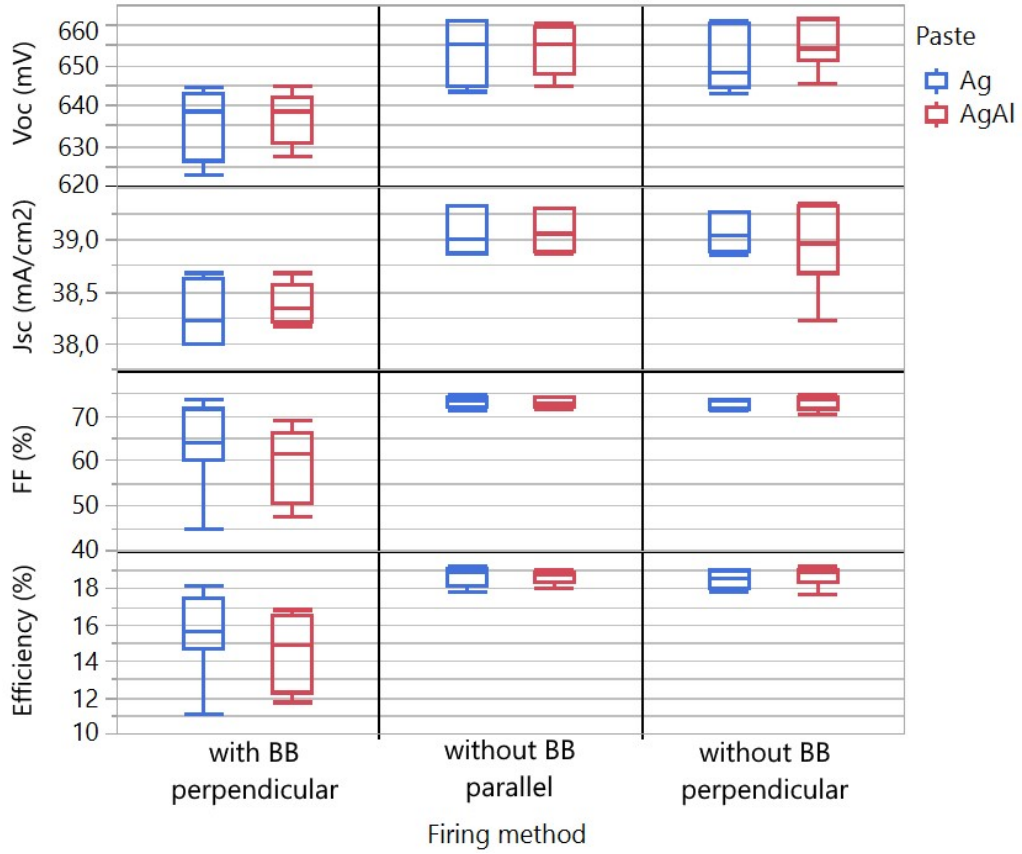

Fig. 40: Solar cell parameters obtained by IV measurement at 25 °C and under AM 1.5 spectrum with illumination intensity of 1000 W/m^2.

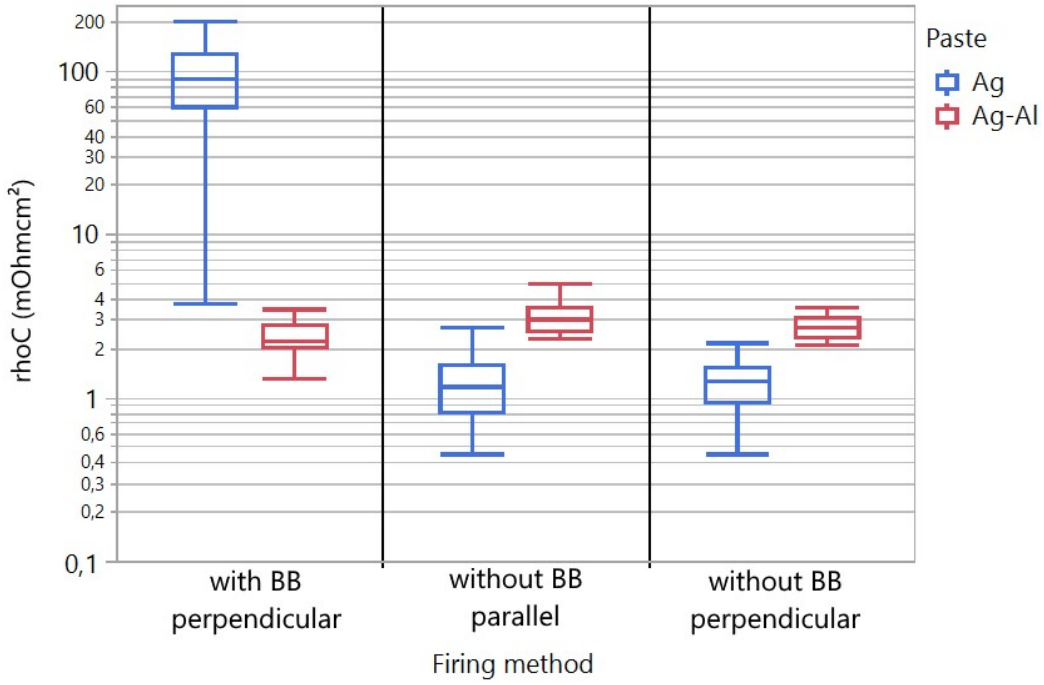

Fig. 41: Contact resistivity ρ_C of Ag and AgAl metallization on boron emitter.

The measured ρ_C of metallization is shown in **Fig. 41**. The best contact (the lowest contact resistivity) was achieved on samples being fired without busbars, independently on the wafer orientation. This is in correlation with the results obtained by IV measurement. Firing with silver printed busbars led to a very high contact resistivity (over 60 mΩcm^2) and it is clearly not suitable for solar cells.

The high values of ρ_C on boron doped surface can depend on the amount of electrons in the doped silicon surface, which plays a key role in the silver-ion reducing reaction [19]. Due to the lack of free electrons in the boron layer, the conditions for creating silver-silicon contact on this surface are much stricter. The use of pure silver paste to contact boron emitter in the combination of low electron concentration and short circuit effect is only possible for firing without busbars. For silver aluminium paste there was no significant difference on contact resistivity between firing with and without busbars.

The results of this work supported the applicability of short-circuit effect in the case of boron emitters. Based on the stated facts, the possibility of printing and firing metallization without busbars was considered. However, high difficulty of contacting non-firing paste on module level forestalled the implementation for the standard process.

CONCLUSION

This dissertation thesis describes newly introduced additional processes and methods for preparation *n*-PERT solar cells and made a useful contribution to clarification and describing connections between the main production steps. Particular influences of production steps were thoroughly considered for the final structure of solar cell. This improved design and to it related adjusted process parameters were put into practice.

Because of using standard production devices not laboratory, the main goal was not to fabricate *n*-PERT cell achieving record efficiency within its category, but to set up all processes to increase the cell efficiency within the ISC Konstanz. Used methods and processes were restricted to those which are designated for industry and allow "cheap" mass-production. Simultaneously, the metal-free process for passivation was preferred to the one containing Al_2O_3.

The newly introduced processes and methods helped to increase the efficiency of the best cell from 20.4 % to 20.9 %. The improvements in other parameters were not negligible, for example V_{OC} from 654 mV to 663 mV, FF from 79.0 % to 80.1 %. For the case of the cheap 6-inch solar cell, produced at standard mass-production line such result could be regarded as sufficient. The J_{SC} slightly decreased from 39.5 mA/cm^2 to 39.3 mA/cm^2. This small decrease can be considered as insignificant because nowadays increasing efficiency of solar cells is mainly connected with increasing of V_{OC} which is technologically much easier than increasing J_{SC}. What concerns other parameters, the iV_{OC} reached 684 mV and J_0 81 fA/cm^2, R_L was reduced below 0.8 Ω/cm. The average value of ρ_C was ranging between 1.25 mΩcm^2 and 3.0 mΩcm^2, depending on wafer orientation during firing and paste composition.

For the proposed *n*-PERT solar cell concept it was necessary to find new ways of diffusion and oxidation processes to obtain the most suitable one for the front surface emitter. The highest efficiency of cell was achieved for the cells with emitter profiles combining low surface carriers concentration and high junction depth. Low carrier surface concentration ensures good surface passivation and its optimal value was found close to $N_{A\ peak}$ ca $2.5 \cdot 10^{19}$ cm^{-3}. The junction depth $d_{emitter} = 0.6$ µm at least contributes to the reduction of contact recombination losses. However, the lowest $J_{0\text{-}met}$ values were obtained for doping profile with high surface carrier concentration. It is necessary to set up the balance between these two opposing requirements very carefully.

The method of wet oxidation was successfully validated as there was a minimal difference in the shape of doping profile and maximal boron concentration between dry and wet oxidation. All low pressure processes showed high quality passivation. Therefore, this method is applicable to the production of *n*-type high efficiency solar cells.

Design and subsequent verification of new optimal structure or passivation layers and antireflection coating was performed and it significantly improved the cell efficiency thanks to reduction of recombination losses while maintaining the light trapping effect. The 10 nm thick layer of SiO_2 is needed as minimum, together with PECVD SiN_X layer with a low refractive index ($n = 2.0$). The passivation degrades if the chemical composition of SiN_X changes towards more Si-rich (higher refractive index), despite the fact that the layer contains more hydrogen, which would have been expected to enhance good passivation. The reason seems to be that, at the same time, the deposition of SiN_X increases the density of interface states, as well as the positive interface fix charges. At combination of SiN_X thickness 84 nm and temperature $\vartheta_{peak} = 780$ °C the contact resistance ρ_C was below 1 $m\Omega cm^2$.

According to literature, the prevention of Potential Induced Degradation (PID) could be solved at the cell level using different composition of ARC and passivation layer, deposited on flat/textured emitter. From the results it is obvious, that the degradation process is related to the degradation of the front side passivation stack layer, where the boron emitter is present. The PID is caused by the enhanced front surface recombination. The type of texturization has no significant influence on degradation on the front side.

Thanks to the in-situ resistance measurement method it was possible to record resistance changes during firing of metallization under different conditions. The temperature required for burning through the dielectric layer was determined from the resistance profile. Using this in-situ method, the differences in behaviour of pure silver and silver-aluminium paste during firing in different process atmospheres were observed.

Contact phenomena are very complex; they are influenced by firing process, by SiN_X thickness, paste composition and by printing scheme. The metallization properties depend primarily on the firing profile and much less on the SiN_X thickness. The metallization induced losses were similar regardless of the paste composition (Ag or AgAl). It was established that pure silver paste can be used for contacting both sides of solar cell instead of silver-aluminium paste for the emitter side and pure silver only for the rear side. Double printed metallization with firing-through paste gives better results than single printed metallization. Separately printed fingers and busbars can increase cell performance, together with right wafer positioning on the belt during firing.

Although the achieved cell efficiency of 20.9 % is, as stated before, in the case of cheap full-size solar cell, produced at standard mass-production line, quite sufficient, there are few other ways for further improvement. One way consists in the field of metallization, including grid pattern and material for metallization allowing easy interconnections between cells on the module level, or point-contacts to minimize resistance losses. Regarding the passivation and ARC layer, it is necessary to establish the optimal composition allowing high quality passivation, easy contacting and preventing PID on the cell level.

ABSTRACT

This dissertation is deals with searching and verifying of new processes contributing towards increase in efficiency of bifacial solar cells based on monocrystalline silicon *n*-type material. This work brings new knowledge about improvements in processes and methods used during its production at the ISC Konstanz. Within this work high efficiency *n*-type PERT (Passivated Emitter Rear Totally diffused) solar cells were made using standard mass-production facilities as in industrial production. This allows to show possibility of production high-quality *n*-type solar cells using almost the same equipment as for *p*-type solar cells. The efficiency increase was based on enhancing and balancing of individual production steps which were the same as in standard mass-production. Experiments described in this work vouch for the improvements in all parts of production of solar cells – improving boron diffusion process or adjusting the passivation layer composition and its properties to new emitter design. Simultaneously, changes in metallization in term of using pure silver paste for emitter metallization, printing layout, and firing sequences were done. The structure and composition of ARC and passivation layer was investigated to reduce the process of Potential Induced Degradation (PID). The highest efficiency of the produced photovoltaics cells based on *n*-type material and made at standard process-line was 20. 9 %.

ABSTRAKT

Tato dizertační práce je zaměřena vývoj a ověřování nových postupů přispívajících ke zvýšení účinnosti bifaciálních solárních článků založených na monokrystalickém křemíku n-typové vodivosti. Tato práce přináší nové poznatky o vylepšených výrobních procesech a postupech použitých během výroby článků v ISC Konstanz. V rámci práce byly vyrobeny solární články typu *n*-PERT (Passivated Emitter Rear Totally diffused) s vysokou účinností, a to pomocí standartních procesů a zařízení používaných běžně při průmyslové výrobě. Zapojení těchto průmyslových postupů a metod umožnilo ověřit možnosti výroby *n*-typových článků za použití téměř totožného vybavení, jaké je potřeba pro výrobu *p*-typových článků. Zvýšení účinnosti bylo založeno především na vylepšení jednotlivých procesních kroků. Experimenty popsané v této práci dosvědčují zlepšení procesu difúze bóru, přizpůsobení parametrů pasivační a antireflexní vrstvy nově navrženému emitoru, zlepšení procesu metalizace ve smyslu využití past neobsahujících hliník, testování tisku rozličných motivů spolu s různými sekvencemi výpalu. V rámci práce byla testována možnost zamezení jevu potenciální indukované degradace (Potential Induced Degradation – PID) pomocí vhodného složení ARC a pasivační vrstvy. Vyrobené n-typové solární články dosáhly maximální hodnoty účinnosti 20,9 %.

REFERENCES

[1] WALSH, C. Solar Cell Efficiency: N-type v. P-type. *CivicSolar* [online]. Austin, USA: CivicSolar, 2017 [cit. 2018-08-01]. Available at: https://www.civicsolar.com/support/installer/articles/solar-cell-efficiency-n-type-v-p-type

[2] SCHMIDT, J. and K. BOTHE. Structure and transformation of the metastable boron- and oxygen-related defect center in crystalline silicon. *Physical review B: Condensed Matter and Materials Physics* [online]. 2004, **62**(2), 241071 - 241078 [cit. 2019-01-28]. DOI: 10.1103/PhysRevB.69.024107. ISSN 2410-3896. Available at: https://link.aps.org/doi/10.1103/PhysRevB.69.024107

[3] GLUNZ, S. W., S. REIN, J. Y. LEE and W. WARTA. Minority carrier lifetime degradation in boron-doped Czochralski silicon. *Journal of Applied Physics* [online]. American Institute of Physics, 2001, **90**(5), 2397–2404 [cit. 2016-02-22]. ISSN 0021-8979. Available at: http://scitation.aip.org/content/aip/journal/jap/90/5/10.1063/1.1389076

[4] MACDONALD, D. and L. J. GEERLIGS. Recombination activity of interstitial iron and other transition metal point defects in p- and n-type crystalline silicon. *Applied Physics Letters* [online]. American Institute of Physics, 2004, **85**(18), 4061–4063 [cit. 2016-02-22]. DOI: 10.1063/1.1812833. ISSN 0003-6951. Available at: http://scitation.aip.org/content/aip/journal/apl/85/18/10.1063/1.1812833

[5] REHMAN, A. and S. H. LEE. Advancements in n-Type Base Crystalline Silicon Solar Cells and Their Emergence in the Photovoltaic Industry. *The Scientific World Journal* [online]. Hindawi Publishing Corporation, 2013, **2013**, 1-13 [cit. 2017-07-06]. DOI: 10.1155/2013/470347. ISSN 1537-744X. Available at: http://www.hindawi.com/journals/tswj/2013/470347/

[6] LIBAL, J. and R. KOPECEK. N-type silicon solar cell technology: ready for take off?. *PV Tech* [online]. London: Solar Media, 2015 [cit. 2017-07-06]. Available at: https://www.pv-tech.org/guest-blog/n_type_silicon_solar_cell_technology_ready_for_take_off

[7] KOPECEK, R. and J. LIBAL. Switch from p to n. *Pv magazine* [online]. 2012, (6) [cit. 2017-07-02]. Available at: https://www.pv-magazine.com/magazine-archive/switch-from-p-to-n_10007072/

[8] Imec develops bifacial n-PERT solar cell with a record 22.8 percent front-side efficiency. *Imec* [online]. Leuven: Imec, 2017 [cit. 2017-05-08]. Available at: https://www.imec-int.com/en/articles/imec-develops-bifacial-n-pert-solar-cell-with-a-record-22-8-percent-front-side-efficiency

[9] CHEN, Z., P. SANA, J. SALAMI and A. ROHATGI. A novel and effective PECVD SiO2SiN antireflection coating for Si solar cells. *IEEE Transactions on Electron Devices* [online]. 1993, **40**(6), 1161-1165 [cit. 2018-03-20]. DOI: 10.1109/16.214744. ISSN 0018-9383. Available at: http://ieeexplore.ieee.org/document/214744/

[10] KRIEG, A., M. GREULICH, J. REIN and S. REIN. Anti-Reflection-Coating Thickness Measurements on Textured Silicon Surfaces: Evaluation and Accuracy of Different Measurement Techniques. In: *28th European Photovoltaic Solar Energy Conference and Exhibition* [online]. München: WIP, 2013, 1820 - 1824 [cit. 2018-03-20]. DOI: 10.4229/28thEUPVSEC2013-2CV.4.56. ISBN 3936338337. ISSN 2196-100X. Available at: https://www.eupvsec-proceedings.com/proceedings?paper=26774

[11] PINGEL, S., O. FRANK, M. WINKLER, S. DARYAN, T. GEIPEL, H. HOEHNE and J. BERGHOLD. Potential Induced Degradation of solar cells and panels. In: *2010 35th IEEE Photovoltaic Specialists Conference* [online]. Honolulu: IEEE, 2010, 2010, s. 002817-002822 [cit. 2017-07-02]. DOI: 10.1109/PVSC.2010.5616823. ISBN 9781424458905. ISSN 2196-100X. Available at: http://ieeexplore.ieee.org/document/5616823/

[12] HALM, A., A. SCHNEIDER, V. D. MIHAILETCHI, L. J. KODUVELIKULATHU, L. M. POPESCU, G. GALBIATI, H. CHU and R. KOPECEK. Potential-induced Degradation for Encapsulated n-type IBC Solar Cells with Front Floating Emitter. *Energy Procedia* [online]. 2015, **77**, 356-363 [cit. 2019-04-01]. DOI: 10.1016/j.egypro.2015.07.050. ISSN 1876-6102. Available at: http://linkinghub.elsevier.com/retrieve/pii/S1876610215008188

[13] STODOLNY, M. K., G. J. M. JANSSEN, B. B. VAN AKEN, et al. PID- and UVID-free n-type Solar Cells and Modules. *Energy Procedia* [online]. 2016, **92**, 609-616 [cit. 2017-07-02]. DOI: 10.1016/j.egypro.2016.07.026. ISSN 1876-6102. Available at: http://linkinghub.elsevier.com/retrieve/pii/S1876610216304532

[14] *IEC TS 62804-1:2015: Photovoltaic (PV) modules - Test methods for the detection of potential-induced degradation - Part 1: Crystalline silicon*. Geneva: International Electrotechnical Commission, 2015.

[15] EDLER, A., V. D. MIHAILETCHI, L. J. KODUVELIKULATHU, C. COMPAROTTO, R. KOPECEK and R. HARNEY. Metallization-induced recombination losses of bifacial silicon solar cells. *Progress in Photovoltaics: Research and Applications* [online]. 2015, **23**(5), 620-627 [cit. 2019-04-01]. DOI: 10.1002/pip.2479. ISSN 1062-7995. Available at: http://doi.wiley.com/10.1002/pip.2479

[16] BÖSCKE, T. S., D. KANIA, A. HELBIG, et al. Bifacial n-Type Cells With >20% Front-Side Efficiency for Industrial Production. *IEEE Journal of Photovoltaics* [online]. 2013, **3**(2), 674-677 [cit. 2017-04-29]. DOI: 10.1109/JPHOTOV.2012.2236145. ISSN 2156-3381. Available at: http://ieeexplore.ieee.org/document/6459517/

[17] KODUVELIKULATHU, L. J., A. EDLER, V. D. MIHAILETCHI, C. COMPAROTTO, A. HALM, R. KOPECEK and K. PETER. Metallization and Firing Process Impact on Voc – A Simulation Study. In: *27th European Photovoltaic Solar Energy Conference and Exhibition* [online]. München: WIP, 2012, **27**, 1432 - 1434 [cit. 2017-07-29]. DOI: 0.4229/27thEUPVSEC2012-2BV.5.33. ISBN 3-936338-28-0. ISSN 2196-100X. Available at: http://www.eupvsec-proceedings.com/proceedings?paper=19920

[18] KIM, H. S., S. B. CHO, H. KIM, D. KIM, M. DOVRAT, G. EYTAN and J. Y. HUH. Electrochemical nature of contact firing reactions for screen-printed silicon solar cells: origin of "gray finger" phenomenon. *Progress in Photovoltaics: Research and Applications* [online]. 2016, **24**(9), 1237–1250 [cit. 2017-03-30]. DOI: 10.1002/pip.2783. ISSN 1099-159X. Available at: https://onlinelibrary.wiley.com/doi/abs/10.1002/pip.2783

[19] KIM, C., J. W. CHOI, S. CHOI, et al. Effects of Current-injection Firing with Ag Paste in a Boron Emitter. *Scientific Reports* [online]. 2016, **6**(1), 21553-21553 [cit. 2017-07-30]. DOI: 10.1038/srep21553. ISSN 2045-2322. Available at: http://www.nature.com/articles/srep21553